Carbon isotope evidence for the latitudinal distribution and wind speed dependence of the air–sea gas transfer velocity

By NIR Y. KRAKAUER[1*], JAMES T. RANDERSON[2], FRANÇOIS W. PRIMEAU[2], NICOLAS GRUBER[3] and DIMITRIS MENEMENLIS[4],   [1]*Department of Earth and Planetary Sciences, University of California, Berkeley, CA 94720, USA;* [2]*Department of Earth System Science, University of California, Irvine, CA 92697, USA;* [3]*Environmental Physics, Institute of Biogeochemistry and Pollution Dynamics, ETH Zurich, Zurich, Switzerland;* [4]*Jet Propulsion Laboratory, Pasadena, CA 91109, USA*

ABSTRACT

The air–sea gas transfer velocity is an important determinant of the exchange of gases, including CO_2, between the atmosphere and ocean, but the magnitude of the transfer velocity and what factors control it remains poorly known. Here, we use oceanic and atmospheric observations of ^{14}C and ^{13}C to constrain the global mean gas transfer velocity as well as the exponent of its wind speed dependence, utilizing the distinct signatures left by the air–sea exchange of $^{14}CO_2$ and $^{13}CO_2$. While the atmosphere and ocean inventories of $^{14}CO_2$ and $^{13}CO_2$ constrain the mean gas transfer velocity, the latitudinal pattern in the atmospheric and oceanic ^{14}C and ^{13}C distributions contain information about the wind speed dependence. We computed the uptake of bomb ^{14}C by the ocean for different transfer velocity patterns using pulse response functions from an ocean general circulation model, and evaluated the match between the predicted bomb ^{14}C concentrations and observationally based estimates for the 1970s–1990s. Using a wind speed climatology based on satellite measurements, we solved either for the best-fit global relationship between gas exchange and mean wind speed or for the mean gas transfer velocity over each of 11 ocean regions. We also compared the predicted consequences of different gas exchange relationships on the rate of change and interhemisphere gradient of ^{14}C in atmospheric CO_2 with tree-ring and atmospheric measurements. Our results suggest that globally, the dependence of the air–sea gas transfer velocity on wind speed is close to linear, with an exponent of 0.5 ± 0.4, and that the global mean gas transfer velocity at a Schmidt number of 660 is 20 ± 3 cm/hr, similar to the results of previous analyses. We find that the air–sea flux of ^{13}C estimated from atmosphere and ocean observations also suggests a lower than quadratic dependence of gas exchange on wind speed.

1. Introduction

In recent decades, the ocean has absorbed roughly one-third of the CO_2 released into the atmosphere by fossil fuel burning (Prentice et al., 2001; Sabine et al., 2004). Ocean CO_2 uptake thus significantly influences the course of greenhouse climate forcing. Further, the added CO_2 makes the ocean more acidic, with likely serious consequences for ocean ecology (Caldeira and Wickett, 2003; Feely et al., 2004a; Orr et al., 2005). As a result, quantitative description of the air–sea CO_2 flux and of changes in ocean carbon chemistry has become a leading goal of oceanographic research (e.g. Fasham, 2003).

The air–sea flux of CO_2 and other gases is generally estimated using a bulk parametrization approach, where the flux is assumed to be proportional to the difference in the concentration of a gas between the bulk ocean and the bulk atmosphere (e.g. Liss and Merlivat, 1986; Frost and Upstill-Goddard, 1999; Orr et al., 2001). This implies a relationship of the form

$$F = k_W \cdot (C_s - C_a), \tag{1}$$

where F is the gas flux out of the ocean (with units such as mol m^{-2} s^{-1}); C_s is the gas concentration in surface water (mol m^{-3}); C_a is the surface ocean concentration of the gas in equilibrium with the partial pressure p (atm) of the gas in the air over the ocean surface computed from Henry's law, that is, $C_a = \alpha \cdot p$, with α (mol m^{-3} atm^{-1}) being the gas solubility; and k_w is an air–sea gas transfer velocity (m s^{-1}) that is independent of the gas concentration but might depend on, for example, the gas

*Corresponding author.
e-mail: niryk@caltech.edu

diffusivity and sea-surface state. In this bulk parametrization, a negative concentration gradient $C_s - C_a$ across the air–sea interface is the driving force for gas uptake by the ocean, but the instantaneous uptake rate for a given concentration gradient depends on the gas transfer velocity k_w.

Accurate knowledge of the gas transfer velocity is needed to estimate contemporary ocean CO_2 uptake from observations of the air–sea pCO_2 disequilibrium (Takahashi et al., 2002) as any bias or uncertainty in the gas transfer velocity leads to a corresponding bias or uncertainty in the flux estimate. The gas transfer velocity is also a very important input parameter for the estimation of the oceanic uptake of anthropogenic CO_2 using an isotopic budget of ^{13}C in the atmosphere and ocean (Tans et al., 1993; Gruber and Keeling, 2001; Quay et al., 2003). Knowledge of the gas transfer velocity is of secondary importance for modelling the air–sea exchange of CO_2, except at regions where vertical mixing is rapid, such as the equator and at high latitudes, where surface water turns over too quickly to reach equilibrium with atmospheric gas pressures (England et al., 1994; Murnane et al., 1999; Ito et al., 2004). Accurate determination of the gas transfer velocity would also help in inferring the air–sea fluxes of a variety of other gases of biogeochemical interest, such as oxygen, nitrous oxide and dimethyl sulfide, from measurements of the concentration gradient across the air–sea interface (e.g. Liss et al., 2004).

Gas transfer velocities over periods of up to a few days have been measured in laboratory wind tunnels as well as in small lakes and in the ocean (overviews in Jähne and Haussecker, 1998; Frost and Upstill-Goddard, 1999). Methods used include eddy correlation for fluxes of gases such as CO_2 (McGillis et al., 2001), and observing the evasion of purposefully released tracer gases such as SF_6 and ^3He (Nightingale et al., 2000). Gas transfer velocities are found to depend on boundary layer turbulence and to be enhanced by the formation of bubbles from breaking waves (see Asher et al., 1998), and often correlate well with prevailing wind speed.

Drawing on such findings, Wanninkhof (1992) proposed a formulation for the air–sea gas transfer velocity as a quadratic function of wind speed,

$$k_W = k_0 \cdot u^2 \cdot (Sc/660)^{-0.5}, \qquad (2)$$

where k_0 is a constant, u is the wind speed measured at 10 m height (m s^{-1}), and Sc is the Schmidt number (water kinematic viscosity divided by the gas diffusivity). The value 660 is a scaling factor included for convenience because it is a typical value for the Schmidt number of CO_2 in the ocean. The exponent -0.5 is representative of the diffusivity dependence found in various laboratory dual-tracer experiments, and more recently also in the open ocean (Nightingale et al., 2000). Wanninkhof (1992) chose the scalar k_0 such that the global mean gas transfer velocity is consistent with the mean gas transfer velocity estimated from natural (Broecker and Peng, 1982) and bomb ^{14}C (Broecker et al., 1986), as we will discuss in the next section.

The Wanninkhof (1992) formulation has been widely adopted for estimating ocean uptake of CO_2 and other gases from an observed or modelled air–sea concentration difference (e.g. England et al., 1994; Orr et al., 2001; Dutay et al., 2002; Takahashi et al., 2002). Earlier, a linear, or piecewise linear, dependence on wind speed was more commonly assumed (Broecker et al., 1985; Liss and Merlivat, 1986; Toggweiler et al., 1989; Tans et al., 1990). Wanninkhof and McGillis (1999) more recently suggested that gas exchange may scale with the cube, rather than the square, of wind speed.

Comparing the commonly used relationships between air–sea gas exchange and wind speed proposed by Wanninkhof (1992), Wanninkhof and McGillis (1999) and others such as Liss and Merlivat (1986) and Nightingale et al. (2000) reveals a range of at least a factor of 2 at any given wind speed. This leads directly to a factor of 2 uncertainty in the air–sea flux when estimated from an air–sea partial pressure difference. The different relationships also lead to rather different diagnosed latitudinal patterns of contemporary air–sea CO_2 fluxes because of the large latitudinal differences in mean wind speed (Fig. 1). As well, if the gas transfer velocity increases as a quadratic or cubic power of wind speed even under high winds, much of the total ocean CO_2 uptake may be occurring during sporadic intense storms, such as hurricanes, and interannual variability in storm frequencies could explain much of the observed interannual variability in the rate of increase of atmospheric CO_2 (Bates, 2002), although inferences from atmospheric O_2 and $\delta^{13}CO_2$ do not support assigning such great interannual variability to the ocean CO_2 sink (Battle et al., 2000). In any case, the discrepancies among the published relationships suggest that formulations of the air–sea gas transfer velocity need further evaluation.

In this study, we explore how observations of ^{14}C and ^{13}C in the atmosphere and ocean can help to constrain the mean gas exchange velocity as well as the exponent of the wind speed dependency. Some of the ^{14}C constraints are well known and have been used previously, but we also introduce new constraints, including the interhemisphere gradient in the atmospheric $^{14}C/^{12}C$ ratio and the rate of decrease in this ratio. We further consider how the measurements of ^{13}C and its air–sea isotope flux can be used to address this question, supplementing the ^{14}C constraints. The next section introduces these constraints and how they have been used in the past.

2. Carbon isotope constraints on the air–sea gas transfer velocity

Observations of ^{14}C (radiocarbon) concentrations in the atmosphere and ocean have played an important role in constraining the gas transfer velocity. ^{14}C is an unstable isotope with a half-life of 5730 yr which comprises about one part in 10^{12} of the carbon in the Earth's atmosphere. ^{14}C is produced in the upper atmosphere at a roughly steady rate in reactions with cosmic rays and solar protons (e.g. Lingenfelter, 1963). From there, it is
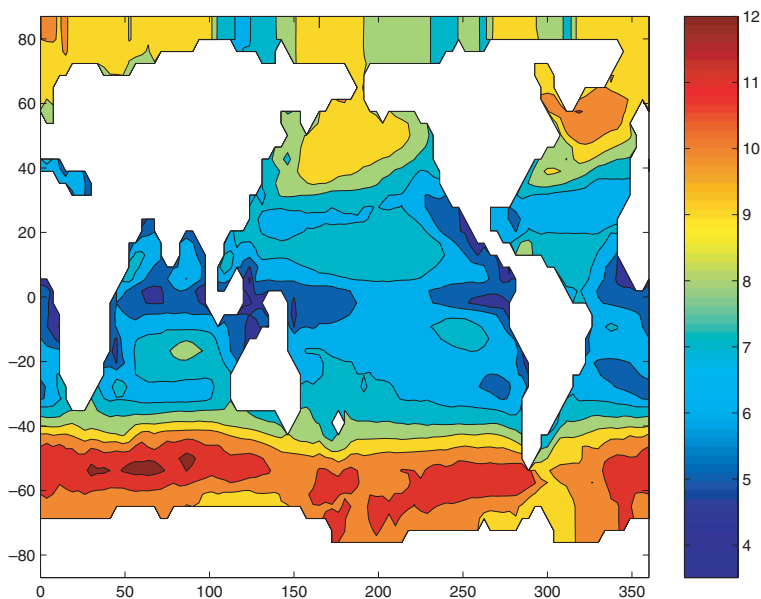
Fig. 1. Annual mean root-mean-square wind speed (m s^{-1}) over the ocean, at 10 m height, from the monthly climatology of Boutin and Etcheto (1997) and Orr et al. (2001), derived from satellite (SSM/I) data. We used the monthly climatology to explore the consequences of different dependences of the air–sea gas transfer velocity on wind speed on ocean ^{14}C uptake. The root-mean-square wind speed varies from 5 to 6 m s^{-1} near the equator to around 11 m s^{-1} over the Southern Ocean.

transported as $^{14}CO_2$ into the lower atmosphere and then taken up by the ocean and terrestrial biosphere. Because water from the deep ocean takes on the order of 1000 yr to circulate to the surface, dissolved inorganic carbon (DIC) in the deep ocean typically has a $^{14}C/^{12}C$ ratio about 200‰ lower than the atmospheric concentration (e.g. Nydal, 2000). Surface ocean DIC reflects exchange both with the deep ocean and with the atmosphere, and so has an intermediate ratio.

The uptake of $^{14}CO_2$ by the ocean is relatively slow. A mixed layer of 50 m depth takes roughly 10 yr for its DIC $^{14}C/^{12}C$ ratio to reach equilibrium with a perturbation in the isotope composition of the CO_2 in the overlying air (Broecker and Peng, 1982). This equilibration timescale is longer than the typical residence time of water in the surface mixed layer, so the ^{14}C level of DIC in the surface ocean can be far from equilibrium with the atmosphere (large concentration gradients across the air–sea interface). This contrasts strongly with the exchange of other gases, including oxygen and chlorofluorocarbons, whose exchange timescale is of the order of a week, resulting in surface ocean concentrations usually being very close to their equilibrium concentration.

^{14}C isotopic abundance is expressed in delta notation, where $\Delta^{14}C$ is the ratio of the measured $^{14}C/^{12}C$ ratio (normalized for mass-dependent isotopic fractionation to a reference $^{13}C/^{12}C$ level) to that of atmospheric CO_2 in the 19th century (determined from tree-ring cellulose carbon), minus one (Stuiver and Polach, 1977). Tree-ring records show that $\Delta^{14}C$ of atmospheric CO_2 (or 'atmospheric $\Delta^{14}C$') remained close to 0‰ in the centuries prior to the 20th century, suggesting that the global carbon cycle remained in an approximate steady-state (Stuiver and Becker, 1993), while measurements of coral carbonate show that surface water DIC averaged around −50‰ (Druffel and Suess, 1983). In the first half of the 20th century, atmospheric $\Delta^{14}C$ dropped by

about 20‰ because of dilution of ^{14}C by CO_2 derived from fossil fuels, which contain no ^{14}C—a drop referred to as the 'Suess effect' (Suess, 1955; Tans et al., 1979; Stuiver and Quay, 1981).

Nuclear bomb tests in the 1950s and early 1960s produced large amount of ^{14}C ('bomb ^{14}C') in the upper atmosphere, so that $\Delta^{14}C$ of CO_2 in the lower troposphere rose to +800‰ by 1964, only to decline in the following decades (to around +65‰ in 2004) as a result of exchange of atmospheric carbon with terrestrial–biosphere and ocean reservoirs that had lower $\Delta^{14}C$ (Fig. 2a). The bomb ^{14}C influx from the atmosphere into the surface ocean increased the $\Delta^{14}C$ of surface water DIC as much as 300‰ by 1970 (Linick, 1980) (Fig. 2b), at a rate set by air–sea gas exchange, and this bomb ^{14}C is now spreading into deeper water (e.g. Broecker et al., 1985; Masiello et al., 1998). Due to the long equilibration timescale of $^{14}CO_2$ across the air–sea interface, ocean bomb $^{14}CO_2$ uptake is strongly limited by air–sea exchange, making the bomb ^{14}C inventory a powerful constraint for the gas transfer velocity.

The first extensive set of measurements of $\Delta^{14}C$ of ocean DIC (or 'ocean $\Delta^{14}C$') was made as part of the Geochemical Ocean Sections (GEOSECS) program. In a series of oceanographic cruises in 1972–1978, $\Delta^{14}C$ profiles were measured at about 100 locations, clearly showing the enhancement of $\Delta^{14}C$ in surface water due to bomb ^{14}C as well as elucidating deep water circulation pathways (Ostlund and Stuiver, 1980; Stuiver and Ostlund, 1980, 1983).

Broecker et al. (1985, 1986, 1995) used the GEOSECS data to estimate the ocean bomb ^{14}C inventory by latitude band, arriving at $305 \pm 30 \times 10^{26}$ atoms in the whole ocean as of the beginning of 1975 (the middle of the GEOSECS program). Based on this inventory, Broecker et al. estimated the global mean CO_2 invasion rate [equivalent to the product $k_w C_a$ in our notation (eq. 1)]

Fig. 2. Representative northern and southern hemisphere observational time-series of $\Delta^{14}C$ for CO_2 in air and for DIC in the upper ocean, showing the bomb ^{14}C spike. (a) Measurements of $\Delta^{14}C$ in atmospheric CO_2 in central Europe (46°–48 °N) (Levin and Kromer, 2004) and in New Zealand (41°S) (G. Brailsford, personal communication, updating Manning et al., 1990), at approximately fortnightly resolution. (b) Measurements of $\Delta^{14}C$ in subtropical (20°–25° N and S) surface coral, at approximately annual resolution. The northern corals are from Florida (Druffel, 1989) and Oahu and French Frigate Reef in Hawaii (Druffel, 1987). The southern corals are from Abraham Reef, Heron Island and Lady Musgrave Island, all in the Great Barrier Reef off Australia (Druffel and Griffin, 1995).
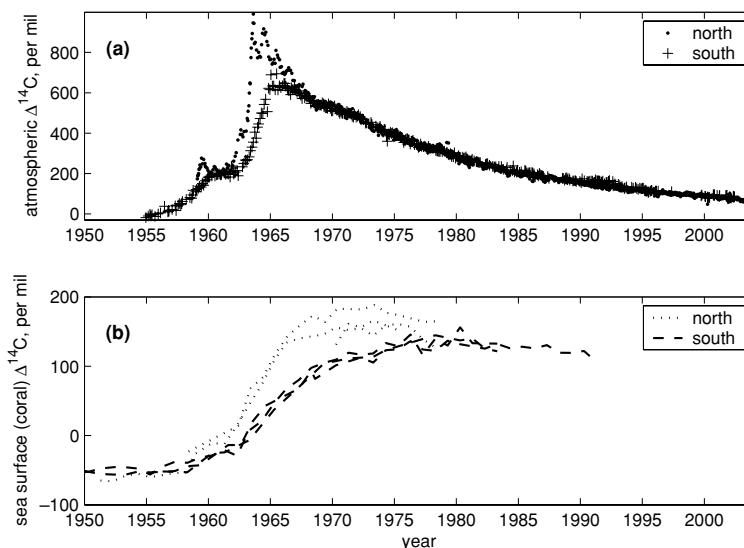
at 20 ± 3 mol m^{-2} yr^{-1} (Broecker and Peng, 1982; Broecker et al., 1986). Broecker and Peng (1982) used GEOSECS and other ^{14}C data to also look at the natural ^{14}C constraint on the gas transfer velocity. This constraint arises from the requirement that at steady state, the net invasion of $^{14}CO_2$ into the ocean must be balanced by the decay of ^{14}C in the ocean. By subtracting the estimated bomb ^{14}C from the observed ^{14}C, Broecker and Peng (1982) obtained estimates of the total ^{14}C content of the ocean in pre-industrial times and of the pre-industrial air–sea difference in $\Delta^{14}CO_2$, from which they derived an estimate of the gas transfer velocity, also with an uncertainty of $\sim$15%. The estimate Broecker and Peng (1982) obtained following this approach was remarkably close to that obtained from the bomb ^{14}C constraint. These ^{14}C-based mean values have since then been widely used (e.g. Tans et al., 1990; Wanninkhof, 1992; Wanninkhof and McGillis, 1999) to set the scaling factor k_0 in expressions for k_w as a function of wind speed (such as eq. 2).

Hesshaimer et al. (1994) attempted to deduce from stratospheric $\Delta^{14}C$ measurements the total amount of bomb ^{14}C produced and to derive a consistent budget for its spread. They found that atmospheric $\Delta^{14}C$ had been declining more slowly than would be expected given the GEOSECS-derived rate of ocean uptake and assumptions about terrestrial biosphere carbon uptake. They, therefore, proposed that mid-1970s ocean bomb ^{14}C uptake had to be $\sim$25% lower, or around 230×10^{26} atoms, and suggested that this implies a lower mean gas transfer velocity.

Peacock (2004) showed that simple extrapolation of the GEOSECS station inventories to the whole ocean likely results in an overestimate of the GEOSECS inventory. She obtained an inventory of $258 \pm 50 \times 10^{26}$ atoms using multiple linear regression of GEOSECS ^{14}C measurements against well-measured ocean quantities, corrected for a systematic bias, and some $270 \pm 25 \times 10^{26}$ atoms for the beginning of 1975 (given as

259–265×10^{26} atoms for the beginning of 1974—we increased this by $\sim$10 $\times 10^{26}$ atoms to obtain an inventory estimate for the beginning of 1975; the uncertainty is given as 'less than 10%') using modelled ocean CFC and anthropogenic CO_2 concentration fields to adjust the Broecker et al. (1995) extrapolation from GEOSECS measurements. This adjustment can be expected to affect the implied mean gas transfer velocity.

In the 1980s and especially the 1990s, the World Ocean Circulation Experiment (WOCE) and affiliated oceanographic survey programs measured ocean $\Delta^{14}C$ at many more locations, increasing the number of available data by an order of magnitude (Key et al., 2002). In this paper, we use both GEOSECS and WOCE data together with an ocean circulation model to evaluate the mean air–sea transfer velocity and the form of its dependence on wind speed implied by ocean bomb ^{14}C uptake. We also revisit the natural ^{14}C constraint developed by Broecker and Peng (1982). In addition, we explore three other ^{14}C constraints, all arising from observations of atmospheric ^{14}C.

The first atmospheric constraint pertains to the pre-industrial interhemispheric gradient of ^{14}C. As a result of the upwelling of very old waters with low $\Delta^{14}C$ in the Southern Ocean, the $^{14}C/^{12}C$ ratio in the surface waters of the Southern Ocean is the lowest anywhere, leading to the largest air–sea gradient in ^{14}C. Taken together with the high wind speeds prevailing in this region, this means that the Southern Ocean takes up a disproportionately large amount of ^{14}C from the atmosphere. This is believed to be the major reason that atmospheric $\Delta^{14}C$ was a few permil lower in the southern than in the northern hemisphere in pre-industrial times, as inferred from measurements of tree rings (Braziunas et al., 1995). This atmospheric gradient is sensitive to latitudinal variation in the air–sea transfer velocity, while the overall rate of pre-industrial ocean ^{14}C uptake is sensitive primarily to the global mean transfer velocity (Broecker and Peng, 1982).

The second and third additional ^{14}C constraints pertain to the post-bomb period. Since the 1980s, the low-latitude oceans have grown close to isotopic equilibrium with the declining atmospheric Δ^{14}C level (e.g. Caldeira et al., 1998), leaving the Southern Ocean, which still has low surface Δ^{14}C due to extensive mixing with deeper waters, as the major site of the uptake of bomb ^{14}C by the ocean (Levin et al., 1987; Randerson et al., 2002). Thus, recent measurements of both the rate of decline in atmospheric Δ^{14}C and the atmospheric Δ^{14}C gradient between the tropics and high southern latitudes should be particularly sensitive to the air–sea gas transfer velocity over the Southern Ocean, providing constraints on the wind speed dependence of the transfer velocity.

We also consider whether what is known about the total global air–sea fluxes of carbon-13 can help in inferring the form of the gas transfer velocity, as suggested by Heimann and Monfray (1989). [13]C has the same slow exchange timescale that characterizes [14]C. This has resulted in the surface ocean ^{13}C/^{12}C ratio lagging substantially behind the recent decrease in the atmospheric ^{13}C/^{12}C ratio arising from the burning of fossil fuels with a low ^{13}C/^{12}C ratio (e.g. Bacastow et al., 1996). As a consequence, there is now a large net ^{13}C isotope flux out of the ocean. However, isotopic fractionation associated with photosynthesis leads to a distinct latitudinal pattern in ^{13}C/^{12}C of ocean DIC, so that there is an isotope flux out of the ocean at low latitudes but into the ocean at high latitudes (Gruber et al., 1999). Thus, given the observed surface ocean ^{13}C/^{12}C ratio of DIC, a stronger increase of the gas transfer velocity with wind speed implies a smaller exchange-weighted ^{13}C isotope flux out of the ocean. This can be compared with the ^{13}C isotope flux required to match observations of the rate of change in the ^{13}C/^{12}C ratio of atmospheric CO_2 and of ocean DIC (Heimann and Maier-Reimer, 1996; Gruber and Keeling, 2001; Quay et al., 2003). A second ^{13}C constraint exists in the steady-state pre-industrial ^{13}C flux, which arises from the input of isotopically light organic carbon by rivers, which is then mostly remineralized in the ocean. This organic carbon flux has been estimated to be about 0.4 Pg C/yr (Heimann and Maier-Reimer, 1996; Aumont et al., 2001). (Of the ~0.7 Pg C/yr entering the ocean via rivers, the remaining ~0.3 Pg C/yr is derived from carbonate dissolution and has a ^{13}C/^{12}C ratio close to that of the ocean, so its contribution to the isotope flux is much smaller and is neglected here.) We compare this steady-state pre-industrial ^{13}C isotope flux with that calculated from the estimated pre-industrial ^{13}C/^{12}C ratio of the atmosphere and of sea-surface DIC; given the strong latitudinal dependence of the air–sea gradient in the ^{13}C/^{12}C ratio, this calculated isotope flux would depend sensitively on the assumed wind speed dependence of the gas transfer velocity.

In combining these multiple carbon isotope constraints, we first present results for simulations of ocean uptake of bomb ^{14}C using an ocean transport model, which we compare with compiled measurements of bomb ^{14}C in the ocean, and with published estimates, based on these measurements, of the total amount and distribution of bomb ^{14}C in the ocean in the 1970s and 1990s (the periods of GEOSECS and WOCE measurements, respectively). Using this evidence, we find the range of global mean transfer velocities and power-law dependences of the transfer velocity on wind speed that best explain the measured distribution. We then check this proposed relationship of the gas transfer velocity with wind speed against other observations of ^{14}C in the atmosphere and of ^{13}C in the ocean and atmosphere. In the comparisons with the observed latitudinal distribution of atmospheric Δ^{14}C, we use an atmospheric transport model to estimate the atmospheric latitudinal gradients that would result from different possible air–sea gas transport patterns. The overall goal of the approaches employed here is to learn from the time evolution of ocean and atmosphere carbon isotope abundances about the mean gas transfer velocity over timescales of months to decades and its regional variability. This would complement smaller-scale laboratory and fieldwork in suggesting and testing parametrizations for air–sea gas exchange.

3. Methods

3.1. Formulation of the air–sea gas transfer velocity

We took as our null hypothesis the parametrization suggested by Wanninkhof (1992), which is scaled to yield the ^{14}C-derived global mean gas transfer velocity and involves a quadratic dependence on wind speed (eq. 2). Following OCMIP Phase 2 (Orr et al., 2001), we used monthly distributions of root-mean-square wind speed derived from Special Sensor Microwave/Imager (SSM/I) satellite measurements of instantaneous wind speed over the ocean, binned into $2.5° \times 2.5°$ boxes and averaged over the period 1988–1993 (Boutin and Etcheto, 1996; Fig. 1) as the basis for estimating u^2. Below, we will refer to this distribution of the gas transfer velocity simply as the Wanninkhof (1992) distribution. The global mean gas transfer velocity implied by this parametrization, averaged over ice-free ocean, is 20.6 cm/hr (at a Schmidt number of 660).

To test whether the Wanninkhof (1992) formulation is consistent with data on air–sea carbon isotope exchange, and to determine, if necessary, a more suitable formulation, we sought to estimate the global mean transfer velocity $\langle k \rangle$ and the wind speed dependence exponent n in the relationship

$$k_W = \langle k \rangle \left(\frac{u^n}{\langle u^n \rangle} \right) (Sc/660)^{-0.5}, \qquad (3)$$

where we used the same root-mean-square climatological SSM/I wind speed (varying spatially and monthly) as an estimate of u and where $\langle u^n \rangle$ is the area-weighted global mean of a power of wind speed (spatially and seasonally constant for a given value of n; for example, if $n = 1$, $\langle u^n \rangle$ would be the global root-mean-square wind speed over the ocean, which for this climatology is 7.82 m s^{-1}). Dividing by $\langle u^n \rangle$ holds the area-weighted global mean transfer velocity at $\langle k \rangle$ regardless of the value of n chosen.
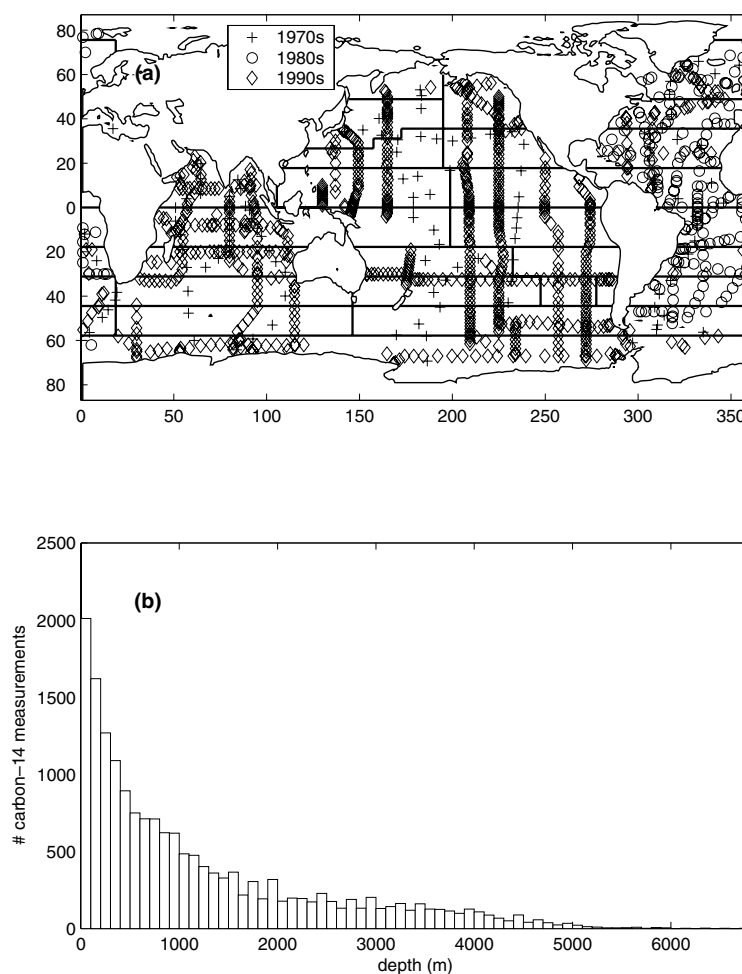
Fig. 3. Distribution of the ocean ^{14}C measurements used in this analysis (Key et al., 2004). (a) Location of measurements, grouped by decade. The 1970s measurements were made as part of GEOSECS, the 1990s measurements mostly as part of WOCE. The thick lines are the boundaries between the 30 ocean regions we use as basis regions for transport pulse functions. (b) Depth distribution of measurements (100 m bins).

To estimate the parameters $\langle k \rangle$ and *n*, we compared the modelled isotope distributions calculated using different values of $\langle k \rangle$ and *n* in eq. (3) with available observations and sought values of $\langle k \rangle$ and *n* that yielded ocean carbon-14 and carbon-13 uptake patterns that agreed well with the observations. We considered values of $\langle k \rangle$ ranging from 0.5 to 1.5 times the Wanninkhof (1992) value, or 10–31 cm/hr, and values of *n* ranging from 0 to 3. As detailed in the following sections, we employed several largely independent approaches, using different sets of observations and different applications of our atmosphere and ocean transport models.

3.2. Estimating the gas transfer velocity from ocean bomb ^{14}C measurements

3.2.1. Ocean circulation model. We simulated the ocean uptake and transport of bomb ^{14}C under different air–sea gas exchange rate scenarios using regional pulse functions derived from the MIT general circulation model (MITgcm) (Marshall et al., 1997). Using a substitute model derived from surface pulse response functions allowed us to efficiently simulate the uptake of bomb ^{14}C for many different scenarios (see Joos (1996) and

Gloor et al. (2001) for the concept). The ocean general circulation model was integrated in a quasi-global (80°S to 80°N) ocean configuration with 1° horizontal grid spacing and with 23 vertical levels, driven by air–sea fluxes of heat, freshwater, and momentum derived by the consortium for Estimating the Circulation and Climate of the Ocean (ECCO) for the 1992–2002 period using the 'adjoint' method to fit the model to a wide variety of satellite and in situ hydrographic observations (Stammer et al., 2004). All configuration details were as in Stammer et al. (2004), except that (i) sea-surface salinity was relaxed to a monthly mean climatology from the National Oceanographic Data Center (NODC) World Ocean Atlas 1998 (WOA98) with a time constant of 30 d and (ii) sea-surface temperature was relaxed to daily mean 1992–2002 estimates from the National Centers for Environmental Prediction and the National Center for Atmospheric Research (NCEP/NCAR) atmospheric reanalysis, also with a time constant of 30 d.

We integrated the MITgcm to obtain pulse-response functions describing concentration patterns resulting from an initial year-long unit pulse of a tracer into each of 30 surface basis regions, uniformly distributed within each region (shown in Fig. 3a). The

resulting concentration fields were saved at monthly resolution for the first 10 yr of each integration and yearly thereafter. Since the model transport varied interannually as driven by the assimilated hydrographic observations from 1992–2002, we calculated pulse functions from each of two nominal starting years (1993 and 1999); the modelled transport from the 1992–2002 period was cyclically repeated. We averaged the two sets of pulse functions to obtain our pulse-function substitute model.

Figure 4a shows the 1994 ocean distribution of the chlorofluorocarbon CFC-11 as simulated by the full MITgcm compared with a gridded compilation of ocean observations from the years centred around 1994 (Key et al., 2004). The ability of a model to reproduce observed ocean CFC uptake patterns is a test of its ability to accurately simulate the transport of bomb ^{14}C, since the two tracers have broadly similar time histories and distribution patterns in the ocean (e.g. Peacock, 2004), having both entered the ocean from the atmosphere over the last few decades. Also, because the CFC concentration at the sea surface equilibrates much more quickly with the changes in atmospheric composition than the ^{14}C abundance, ocean CFC distributions are relatively insensitive to variation in the air–sea gas transfer velocity. Thus, model-data discrepancies in CFC concentrations are an indicator of model transport error, whereas model-data discrepancies in bomb ^{14}C abundance could be due either to transport error or to error in the specified gas transfer velocity. Boundary conditions for the simulation followed the OCMIP protocol for chlorofluorocarbons (Dutay et al., 2002), and we used the Wanninkhof (1992) air–sea gas exchange formulation, that is, eq. (2) with SSM/I climatological winds. The model-data comparison shows that MITgcm simulates the ocean CFC inventory and its latitudinal distribution reasonably accurately, suggesting that we might be able to use the mismatch between the modelled and observed ocean bomb ^{14}C distribution to learn about air–sea gas transfer. In fact, the configuration of MITgcm used here has been found to reproduce CFC concentrations measured during the 1990s WOCE cruises better than any of the other ocean models compared in a recent study (Mikaloff Fletcher et al., 2006); the correlation coefficient between individual ocean CFC measurements in the GLODAP database and the modelled CFC concentration at the same grid box and month was +0.92.

To validate using the pulse function substitute model instead of the full MITgcm transport to simulate ocean bomb ^{14}C uptake, we conducted a single simulation of bomb ^{14}C uptake using the full MITgcm (with the Wanninkhof (1992) air–sea gas exchange formulation, and with boundary conditions otherwise as below) and compared it with a simulation of bomb ^{14}C uptake using the substitute model. Compared with the full model, the pulse function substitute model represented reasonably well the time evolution of the ocean bomb ^{14}C inventory (Fig. 4b) and its latitudinal distribution (Figs. 4c and d). The correlation coefficient between the two runs of bomb Δ^{14}C at the grid cells and months where measurements were available was +0.97.
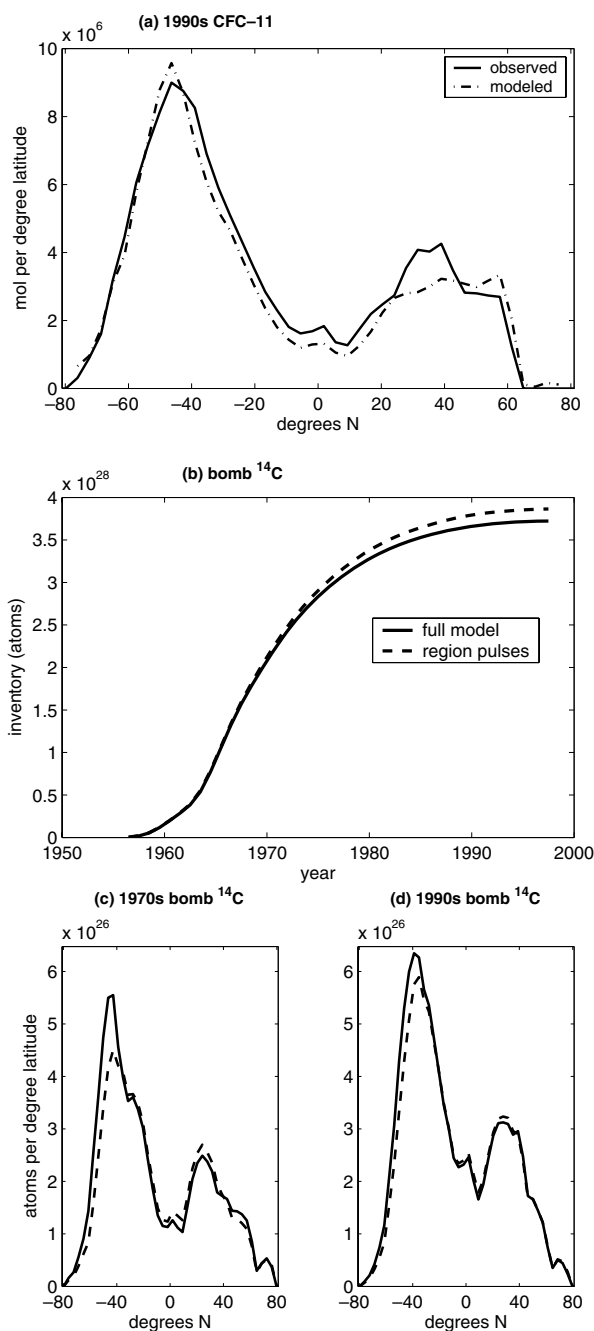

Fig. 4. (a) Modelled (MITgcm) 1994 latitudinal distribution of the chlorofluorocarbon CFC-11, compared to a gridded distribution based on observations (Key et al., 2004). The modelled distributions are summed only over the grid cells for which the gridded distribution is available, largely excluding, for example, the Arctic Ocean. The corresponding modelled global inventory is 4.82×10^8 mol, compared with $(5.16 \pm 0.8) \times 10^8$ mol estimated from observations. (b–d) Ocean bomb ^{14}C modelled using the full MITgcm transport fields as compared with our pulse function substitute model: (b) shows the time history of the ocean inventory, and (c) and (d) show the latitudinal distribution of the ocean inventory in 1975 and 1994, respectively. The legend for (c–d) is the same as that for (b).

3.2.2. Simulating air–sea exchange of bomb ^{14}C. Following the simplified formulation of Toggweiler et al. (1989), we carried bomb ^{14}C in Δ units, and it entered the surface layer following a version of eq.(1) appropriate for isotope fluxes, namely

$$F = k_W \cdot \alpha \cdot \big\{ (pCO_2/DIC) \cdot \big(\Delta_{sea}^{14}C - \Delta_{air}^{14}C \big)$$
$$+ [(pCO_2/DIC) - (pCO_2/DIC)_{pre-bomb}]$$
$$\cdot \big(\Delta_{sea}^{14}C - \Delta_{air}^{14}C \big)_{pre-bomb} \big\}, \tag{4}$$

where F is now the air–sea flux in Δ units m s^{-1} (positive when out of the ocean), k_w is the gas transfer velocity for CO_2 in m s^{-1}, α is the solubility of CO_2 in seawater (mol m^{-3} atm^{-1}), $p CO_2$ is the partial pressure of CO_2 in the air (atm), and DIC is the sea-surface DIC concentration (mol m^{-3}). In the first term, $\Delta_{sea}^{14}C$ is the bomb carbon-14 content of sea-surface DIC in Δ units, $\Delta_{air}^{14}C$ is the carbon-14 content of atmospheric CO_2 in Δ units above the pre-industrial level of 0‰, and the driving force for flux into the ocean is the increased $\Delta_{air}^{14}C$ due to bomb ^{14}C production. In the second term, $(\Delta_{sea}^{14}C - \Delta_{air}^{14}C)_{pre-bomb}$ refers to the pre-bomb air–sea $\Delta^{14}C$ gradient, and the driving force is the increase in the atmospheric CO_2 partial pressure due to fossil fuel burning, which increases the flux of ^{14}C into the ocean even with unchanged $\Delta_{air}^{14}C$ (Joos and Bruno, 1998). The effect of this second term is much smaller than that of the first term for the GEOSECS period, because $(\Delta_{air}^{14}C - \Delta_{sea}^{14}C)$ was very large then and the CO_2 elevation ($p CO_2 - p CO_{2 pre-bomb}$) was small, but its relative importance increases by the 1990s.

We computed the uptake of bomb ^{14}C by the ocean by combining the flux boundary condition (eq. 4) with the substitute model representing the transport of bomb ^{14}C into the ocean interior. Our bomb ^{14}C simulations began in 1956 with an ocean bomb ^{14}C concentration initialized at zero (following the operational definition of bomb ^{14}C used in Rubin and Key (2002)) and then stepped forward in time.

Of the terms on the right-hand side of eq. (4), we varied k_w as specified below. $\Delta_{sea}^{14}C$ was the model prediction for the end of the previous time step. Values for the other terms were adapted from those used in various OCMIP tracer uptake studies, as follows. The value α was calculated based on the relationship of Weiss and Price (1980) and monthly climatological water surface temperature and salinity from the World Ocean Atlas 2001 (Boyer et al., 2002; Stephens et al., 2002). pCO_2 was estimated from a time-series of annual mean CO_2 mixing ratios based on measurements at Mauna Loa (http://quercus.igpp.ucla.edu/OceanInversion/inputs/atm_co2/splco2_mod.dat; updated from Keeling et al., 1976) multiplied by a monthly climatology of sea-level atmospheric pressure from Esbensen and Kushnir (1981). [Strictly speaking, the CO_2 mixing ratios are expressed as fractions of *dry* air, so that pCO_2 here is slightly higher than the actual CO_2 partial pressure. This is compensated for in the solubility constant α, assuming that air at the sea surface is saturated with

water vapour (Weiss, 1974).] $\Delta_{air}^{14}C$ was from a compilation of annual mean values for northern, equatorial and southern latitudes (I. Levin, personal communication to J. Orr, http://www.ipsl.jussieu.fr/OCMIP/phase3/simulations/NOCES /boundcond/atmC14/Levin/Jim_data_2004.doc, henceforth: Levin, unpublished) based on long-term atmospheric measurement series at several sites (e.g. Rozanski et al., 1995; Levin and Kromer, 2004). DIC was based on climatologies produced by the Global Ocean Data Analysis Project (GLODAP) for the 1990s (from extensive oceanographic observations) and pre-industrially [by subtracting an estimated anthropogenic component from the observations (Gruber et al., 1996; Key et al., 2004)]. We interpolated between the pre-industrial period and the 1990s by assuming that the amount of anthropogenic DIC in the ocean is everywhere proportional to the atmospheric CO_2 mixing ratio elevation above the pre-industrial level at the current time step. The comparatively small share of anthropogenic DIC during the simulation period (generally less than 3% of total DIC, even at the surface) means that the error resulting from this simplifying assumption is small.

Our formulation (eq. 4) assumes that at the beginning of the simulation period, the ocean $\Delta^{14}C$ distribution was at approximate steady state with an atmospheric $\Delta^{14}C$ of 0‰. This is clearly not completely true, because of the pre-bomb decline in ocean $\Delta^{14}C$ (the Suess effect), the effect of early bomb explosions prior to 1956 in increasing $\Delta^{14}C$ (which partially cancels out the Suess effect), and changes in ocean circulation and in the cosmogenic ^{14}C production rate over timescales up to that of ocean mixing ($\sim$1000 yr). Rubin and Key (2002) found no detectable trend from 1945 to 1955, just prior to the start of our simulation period, in a surface coral $\Delta^{14}C$ dataset with a standard deviation of 7‰, suggesting that the error incurred by this steady-state assumption is of the same order or smaller then the bomb component separation error of 13‰ (and much smaller than the mean 1970s surface bomb $\Delta^{14}C$ elevation of $\sim$160‰).

We applied eq. (4) to ice-free water. We assumed that no gas exchange occurs across sea ice, defined by a monthly sea ice climatology based on Walsh (1978) and Zwally et al. (1983).

3.2.3. Data-model comparison. We took two different approaches for varying the Wanninkhof (1992) gas transfer velocity to fit ocean bomb ^{14}C observations. In the first approach, we fit the air–sea exchange parameters $\langle k \rangle$ and n (in eq. 3) to bomb ^{14}C observations. We simulated ocean bomb ^{14}C uptake for different values of $\langle k \rangle$ and n on a mesh using a spacing of 0.1 times the Wanninkhof (1992) value (or about 2 cm/hr) in $\langle k \rangle$ and 0.3 in n. We solved for the best-fit values of $\langle k \rangle$ and n by linearizing a misfit function that gave a measure of the discrepancy between available measurements of bomb ^{14}C (discussed below) and model predictions of bomb $\Delta^{14}C$ at the same times and places. In our second approach, we solved for the best-fit mean transfer velocity in each of 11 large ocean regions, which were aggregations of the 30 ocean regions for which we had pulse functions and

were very similar to the basis regions of the TransCom study (Gurney et al., 2002). We successively perturbed the transfer velocity for each region from the Wanninkhof (1992) global mean by a fractional amount (generally 0.1) to construct a linear operator that represented the effect of varying the mean gas transfer velocity in each region on the amounts of bomb ^{14}C simulated at the measurement locations and months. This linearization made it easier to estimate the regional transfer velocities that minimized the misfit between simulated and observed values. Since the non-linearity of the dependence of simulated concentrations and inventories on the air–sea transfer velocity was weak, iterating this linearization about the regional transfer velocities estimated from the previous iteration led to rapid convergence. This approach is conceptually similar to that of Gloor et al. (2001; 2003) and Gruber et al. (2001), who solved for regional air–sea fluxes of heat, oxygen, or anthropogenic CO_2 that best-fit ocean observations. We fit a power law to the relationship of our derived regional gas transfer velocities with regional mean wind speeds to obtain another estimate of the globally optimal values for $\langle k \rangle$ and n.

We compared our simulated bomb ^{14}C fields with a quality-controlled compilation of 17,501 measurements of ^{14}C in ocean water samples prepared by the Global Ocean Data Analysis Project (GLODAP) (Key et al., 2004), which represent 1070 depth profiles (Fig. 3). The compilation includes measurements from GEOSECS in the 1970s and from several cruises in the 1980s, with a predominance of measurements from the WOCE program in the 1990s. A measurement of an ocean sample taken in the 1970s–1990s reveals only its total Δ^{14}C. To compare this measurement to a simulated value of bomb Δ^{14}C requires an estimate of the water's 1950s (pre-bomb) Δ^{14}C, which can be then subtracted to yield the bomb enhancement. For most of the ocean Δ^{14}C measurements, GLODAP provides estimates of this background level and of the bomb enhancement component. These are based primarily on the assumption that the water's pre-bomb Δ^{14}C is linearly related to its potential alkalinity. Water with higher potential alkalinity has generally been in the deep ocean longer, and thus had lost ^{14}C to decay. This relationship was calibrated using 1950s coral and surface water samples, as well as more recent deep water samples that still contain little bomb ^{14}C (Rubin and Key, 2002). The typical error in deducing Δ^{14}C from potential alkalinity is found to be around 12‰ (Rubin and Key, 2002). This is much worse than the analytical precision of the Δ^{14}C measurements, typically around 5‰ (Key et al., 2002).

An alternative estimate of the Δ^{14}C background, with roughly the same accuracy, is based on the water silica content: water high in silica tends to have low background Δ^{14}C (Broecker et al., 1985; Broecker et al., 1995; Peacock, 2004). We calculated bomb ^{14}C values using this method as well, employing silica measurements for the same water samples (also from the GLODAP compilation) and the relationship between silica and background Δ^{14}C derived by Peacock (2004). As a check on the sensitivity of our fit to the bomb ^{14}C component separation, we used both these silica-based determinations of bomb Δ^{14}C and the GLODAP ones, which are based primarily on potential alkalinity.

Given the observational estimates of bomb Δ^{14}C at the measured locations and times, we constructed a misfit function which consisted of the summed discrepancy between bomb ^{14}C levels in individual measurements, or alternatively column inventories (the integrals of measured bomb ^{14}C depth profiles), and model-predicted levels for the same months and grid cells, using data from either the GEOSECS period (1970s) or the WOCE period (1980s-1990s). Many more measurements are available from the 1990s, but because much more time has passed since the period of fastest ocean bomb ^{14}C uptake (∼30 yr as opposed to ∼10 yr in the 1970s), the effect of transport errors on attributing source regions to the observed ^{14}C distribution could well be larger.

For either the 1970s or the 1980s–1990s observations, we thus determined which regional gas transfer velocities, or which global mean and wind speed dependence of the gas transfer velocity, minimized the overall misfit between the observations and model predictions. For simplicity, and pending more detailed analysis of the statistics of the measurement, bomb-component separation, and model-transport errors, we assumed the error of each measurement or column inventory to be the same, meaning that all observations or column inventories were weighted equally.

In standard least-squares optimization, the sum of the squared observed-modelled discrepancies (the 2-norm) is minimized; this minimum is easy to compute and is theoretically the maximum-likelihood estimate of the model parameters if the remaining errors have a Gaussian distribution with the assumed covariance matrix. In our comparisons we found that there are often more extreme values in the modelled-measured residual than in a Gaussian distribution, as occasional unusually large modelled-measured misfits result from, for example, a bomb ^{14}C measurement made below the thermocline at a depth that in the model was above the thermocline and hence had a much higher predicted bomb ^{14}C content. Minimizing a 2-norm would lead to these outlying measurements unduly influencing the best-fit parameter values, so we have preferred to calculate minimum misfits using the 1-norm (i.e. the sum of the absolute values of the differences between observed and simulated concentrations), which should be more reliable in the presence of outliers (e.g. Aster et al., 2005, Section 2.4). We estimated 1 standard deviation uncertainty ranges for the 1-norm minimum from the curvature of the misfit function near its minimum (where it can be approximated as a parabola) using the results of Parker and McNutt (1980). However, we found that the variation in the optimum parameter values among an ensemble of misfit functions where either individual measurements or column inventories, and either potential-alkalinity or silica-based observational bomb-^{14}C estimates, were matched, was often larger than this uncertainty, which, for example, optimistically assumes that transport errors

are uncorrelated between measurements; where this was the case, we used the standard deviation of this ensemble of misfit functions instead as a more accurate indication of the uncertainty of our results.

Several efforts have been made to extrapolate from the GEOSECS ^{14}C measurements the amount of bomb ^{14}C present in the mid-1970s in each latitude band of the ocean (Broecker et al., 1995; Peacock, 2004). As part of GLODAP, gridded maps of ocean total and bomb ^{14}C were also developed based on interpolation from WOCE-era measurements (Key et al., 2004). To get an overall picture of how changing the air–sea gas transfer velocity changes the modelled ocean bomb ^{14}C as compared with observed bomb ^{14}C levels, we also plotted our simulated global bomb ^{14}C ocean total and its latitudinal distribution for the mid-1970s and mid-1990s (at the middle of the GEOSECS and WOCE periods, respectively) compared with these observation-based inventories.

3.3. Atmospheric evidence for 1990s ocean ^{14}C uptake

Key et al. (2004) used extensive ocean Δ^{14}C surface measurements to construct a sea-surface Δ^{14}C climatology for the WOCE period (centred around 1994). From this GLODAP climatology and eq. (4), we computed the expected latitudinal gradient in Δ^{14}C of atmospheric CO_2 for different wind speed dependences of air–sea gas exchange, without reference to an ocean circulation model. To do this, we had to account for contributions to the latitudinal gradient from cosmogenic production, fossil fuel burning, and terrestrial biosphere respiration. We assumed that long-term cosmogenic production averages 6.2 kg ^{14}C/yr, balancing decay in short-term carbon pools (Goslar, 2001) and consistent with observed ^{14}CO concentrations (Quay et al., 2000), and that interannual variability in production is proportional to the sunspot number (Lingenfelter, 1963). Carbon from fossil fuels contains no ^{14}C, and so the concentration of fossil fuel burning in the northern mid-latitudes results in $\Delta^{14}CO_2$ depletion in the northern hemisphere (Levin et al., 2003). We modelled this surface flux using distributions of fossil CO_2 emissions from Andres et al. (1996). Also, most of the respired biomass in the 1990s was fixed when the atmosphere contained more bomb ^{14}C, with the result that since the 1980s, land biosphere respiration has been a net source of ^{14}C. This ^{14}C-enriched flux is highest in the tropics and in the north temperate zone where net primary production is high (Randerson et al., 2002). We modelled this flux using spatially and seasonally resolved biomass respiration pulse functions derived from the CASA biosphere model (Thompson and Randerson, 1999) convolved with the atmospheric Δ^{14}C history.

To predict the gradients in atmospheric Δ^{14}C resulting from various air–sea gas exchange patterns combined with other carbon fluxes, we again used regional pulse functions for their computational speed and accuracy. These atmospheric pulse response functions, which compactly represent the effect of the release of

Table 1. Rate of decline of atmospheric Δ^{14}C around 1994

Station	Δ^{14}C of atmospheric CO_2 (‰)			Rate of decline (‰/yr)
	Latitude	1992.0[d]	1997.0[d]	
Schauinsland[a]	48°N	138	102	7.2
Jungfraujoch[a]	47°N	139	105	6.8
Pretoria[b]	26°S	148	117	6.3
Wellington[c]	41°S	153	114	7.7
Mean ± SD				7.0 ± 0.6

[a]Levin and Kromer (2004).
[b]S. Woodbourne, personal communication, updating Manning et al. (1990).
[c]G. Brailsford, personal communication, updating Vogel (1971).
[d]For the northern hemisphere stations, calculated as the average of the preceding and subsequent summer (since atmospheric Δ^{14}C near the surface is more variable in winter than in summer).

a unit amount of inert tracer at the surface in a particular region on the atmospheric concentration pattern of that tracer (e.g. Randerson et al., 2002), were generated using the Model of Atmospheric Transport and Chemistry (MATCH) (Mahowald et al., 1997). MATCH was run with approximately 5.5° horizontal resolution and 26 vertical levels, and driven by meteorological fields from the NCAR Community Climate Model Version 3 (Olsen and Randerson, 2004). Our pulse functions corresponded to tracer releases over the 22 TransCom regions (Gurney et al., 2002) over each month of the year, allowing us to accurately represent seasonally varying fluxes. We also constructed pulse functions for northern, southern, and equatorial tracer release in the stratosphere (at the 90 millibar pressure level) and in the upper troposphere (at 200 millibar) to allow us to simulate the effect of cosmogenic ^{14}C production in the upper atmosphere on atmospheric Δ^{14}C gradients.

To estimate the error in modelling atmospheric transport with our pulse functions, we compared the latitudinal Δ^{14}C gradients modelled for several of our flux fields with those predicted by annual mean regional pulse functions generated from an ensemble of 15 transport models for the TransCom Level 3 experiment (Gurney et al., 2003). Our model predictions were generally within one standard deviation of the intermodel mean. We used the intermodel standard deviation as an estimate of the error in the predicted gradients induced by our atmospheric transport model.

There has been significant interannual variability in the rate of decline of the Δ^{14}C of atmospheric CO_2 (e.g. Levin and Kromer, 2004). We estimated this rate of decline as 7.0 ± 0.6‰/yr for a 5 yr period centred around 1994 by taking the average of available long-term atmospheric Δ^{14}C measurement series (Table 1). We estimated the contributions of the major influences on the atmospheric $^{14}CO_2$ isotopic budget (Table 2) and calculated the dependence of the ocean uptake on the parameters $\langle k \rangle$ and n.

Table 2. Modelled contributions of carbon fluxes to the rate of decline and latitudinal gradient in atmospheric Δ^{14}C around 1994

	Growth rate (‰/yr)	Latitudinal gradient[a] (‰)
Biosphere[b]	3.7 ± 0.7	2.7 ± 1.2
Fossil fuels[b]	-9.3 ± 0.5	-7.8 ± 1.6
Cosmogenic production[b]	6.2 ± 0.6	0.5 ± 0.6
Ocean		
Linear[c]	-8.2 ± 0.6	8.9 ± 2.6
Quadratic[c]	-9.3 ± 0.7	12.2 ± 3.4
Cubic[c]	-10.3 ± 0.7	15.4 ± 4.3
Model uncertainty[d]	± 1.3	± 3.5
Measured value	-7.0 ± 0.6[e]	5.6 ± 2.8[f]
Total uncertainty[g]	± 1.4	± 4.5

[a]Annual mean Δ^{14}C at Llano de Hato, Venezuela (9°N), subtracted from that at Macquarie Island (54°S).

[b]Modelled effects (see Methods section); 1-SD uncertainties reflect approximate confidence in flux size, plus error in the atmospheric transport model (estimated from the spread in standardized regional pulse functions of models participating in the TransCom 3 intercomparison (Gurney et al., 2003)) in the case of the latitudinal gradient.

[c]For air–sea gas transfer velocity formulations with the global mean rate the same as in the OCMIP formulation ($\langle k \rangle = 20.6$ cm/hr in eq. 3) and a linear, quadratic, or cubic dependence on wind speed ($n = 1, 2$ or 3). The given uncertainties reflect confidence in the air–sea Δ^{14}C disequilibrium and in the atmospheric transport model, assuming that the given formulation of gas exchange is correct.

[d]Overall uncertainty in the model prediction: sum of the uncertainties from the different components, assuming the quadratic dependence of air–sea gas exchange on wind speed for the ocean contribution.

[e]See Table 1.

[f]Levin and Hesshaimer (2000).

[g]Model plus measurement uncertainty contributions.

Uncertainty in several other contributions to the rate of decline was also around 0.6‰/yr (Table 2), and summing their contributions to the error variance yielded a total uncertainty of ± 1.4‰/yr for the model-data comparison.

Published data on the latitudinal distribution of atmospheric Δ^{14}C in the 1990s are scarce. ^{14}C uptake in the Southern Ocean is the major influence on the Δ^{14}C gradient between the tropics and high southern latitudes, while Δ^{14}C gradients in the northern hemisphere are dominated by the influence of fossil carbon emissions (e.g. Levin et al., 2003). We compared the mean difference of 5.6 ± 2.8‰ observed for 1993–1994 between Llano de Hato, Venezuela (9°N) and Macquarie Island in the Southern Ocean southeast of Australia (54°S) (Levin and Hesshaimer, 2000) to that predicted by our atmospheric transport model for different air–sea gas exchange parameter values after accounting for the effect of other exchange processes (Table 2). Uncertainty in the predicted gradient due to model transport is about

the same size as the reported measurement error but varies depending on the absolute size of the predicted gradient; the total uncertainty for the model-data comparison was about 4.5‰ (Table 2).

3.4. Pre-industrial ocean ^{14}C uptake

We modelled air–sea ^{14}C fluxes using eq. (4), an atmospheric Δ^{14}C level of 0‰, and the GLODAP climatology of estimated pre-bomb ocean surface Δ^{14}C (Key et al., 2004), which we adjusted by using a simulation with the MOM ocean circulation model (Primeau, 2005), run with the OCMIP air–sea gas transfer velocity and a time-series of the change in atmospheric Δ^{14}C between 1850 and 1955 compiled from tree-ring measurements (Stuiver and Quay, 1981) (Levin, unpublished), to estimate the small depletion attributable to pre-bomb fossil fuel dilution (the Suess effect).

The total amount of ^{14}C in the pre-industrial ocean can be determined to an accuracy of perhaps 2% by integrating the pre-bomb ^{14}C distribution estimated by GLODAP and making a small correction for the effect of fossil fuel CO_2 to 1956. To estimate the pre-industrial air–sea ^{14}C flux, one could assume steady state and take the net flux into the ocean to match the decay of ^{14}C in ocean DIC; this amount is 5.4 kg ^{14}C (2.3×10^{26} ^{14}C atoms) per year. Broecker and Peng (1982) estimated that the pre-industrial ocean-surface Δ^{14}C is known to $\sim$10‰, leading to an uncertainty of $\sim$15% in the deduced global mean gas transfer velocity. The assumption of steady state is open to question, however, since it fails to account for exchange of DIC with other carbon pools with low Δ^{14}C, such as carbonate and organic sediment and volcanic or hydrothermal CO_2; the magnitude of this exchange is poorly known (Damon and Sternberg, 1989; Goslar, 2001). For example, an input of 0.5 Pg per year of carbon containing essentially no ^{14}C would increase the steady-state air–sea flux required by 0.3 kg ^{14}C/yr, or $\sim$6%. (By comparison, net sedimentation of carbonates is estimated at 0.2 Pg C/yr, and volcanic or hydrothermal releases into the ocean at 0.1 Pg C/yr (Aumont et al., 2001).) In addition, some deviation from steady state flux, caused for example by long-term oscillations in the atmospheric ^{14}C production rate (Lingenfelter, 1963) or in ocean circulation, is possible. Allowing for these uncertainties, we estimated the pre-industrial air–sea flux at 5.4 ± 1 kg ^{14}C/yr and compared it with that predicted for different values of $\langle k \rangle$ and n.

The pre-industrial interhemispheric Δ^{14}C gradient has been carefully measured (with replicate northern and southern samples analysed in two laboratories to eliminate intercalibration error) as the offset in cellulose Δ^{14}C between tree rings from Britain and New Zealand (Hogg et al., 2002). Some oscillation over decade to century periods was found, with a mean $\pm$ standard deviation of 4.8 ± 1.6‰ over the period 950–1850. (From earlier tree-ring measurements, Braziunas et al. (1995) estimated a similar pre-industrial gradient of 4.4 ± 0.5‰

Table 3. Deriving the ^{13}C isotope flux out of the ocean around 1995 from the atmospheric ^{13}C budget

Observed or estimated quantities		
Atmospheric CO_2	$763.8^a \pm 3.2$	Pg C
Fossil CO_2 emissions	$6.4^b \pm 0.3$	Pg C/yr
Ocean anthropogenic CO_2 uptake	$2.2^c \pm 0.3$	Pg C/yr
Atmospheric CO_2 rate of increase	$3.2^d \pm 0.3$	Pg C/yr
Mean $\delta^{13}C$ of fossil emissions	-28.1 ± 1	‰
Mean $\delta^{13}C$ of atmospheric CO_2	$-7.91^e \pm 0.03$	‰
Disequilibrium of terrestrial respiration	$0.35^f \pm 0.1$	‰
Terrestrial net primary productivity	$55.4^f \pm 15$	Pg C/yr
Terrestrial photosynthesis ^{13}C discrimination	-19 ± 1.5	‰
Rate of change in $\delta^{13}C$ of atmospheric CO_2	$-0.018^e \pm 0.005$	‰
River flow of terrestrial organic matter into ocean	$0.4^g \pm 0.2$	Pg C/yr
Derived quantities		
Land biosphere CO_2 uptake	1.0 ± 0.5	Pg C/yr
Atmospheric ^{13}C budget: isotope fluxes		
Fossil fuels	-128 ± 9	Pg C ‰/yr
Land biosphere, from isotopic disequilibrium	19 ± 8	Pg C ‰/yr
Land biosphere, from fractionation in net CO_2 uptake	18 ± 10	Pg C ‰/yr
Storage in atmosphere (change in $\delta^{13}C$)	-14 ± 4	Pg C ‰/yr
Inferred air–sea isotope flux (relative to a pre-industrial steady state)	77 ± 16	Pg C ‰/yr
Air–sea isotope flux to balance river flow at steady state	-8 ± 4	Pg C ‰/yr
Inferred total air–sea isotope flux	70 ± 17	Pg C ‰/yr

Adopted values and 1-SD uncertainties were mostly based on those used in the similar calculations by Heimann and Maier-Reimer (1996) and Gruber and Keeling (2001), except as specified below.
[a]From 1995 means of NOAA-CMDL flask measurements (Conway et al., 1994) for remote stations, binned by latitude and averaged.
[b]Marland et al. (2005)
[c]Mikaloff Fletcher et al. (2006)
[d]Change over the 1990s in NOAA-CMDL flask measurements (Conway et al., 1994) for remote stations, binned by latitude and averaged.
[e]1995 means and change over the 1990s in measurements from the CSIRO (Francey et al., 2001) and Scripps (Keeling et al., 1995) station networks, binned by latitude and averaged.
[f]CASA (Potter et al., 1993) plant and soil carbon model; the disequilibrium was derived by weighting respiration pulse functions from CASA (Thompson and Randerson, 1999) with a time-series of change in atmospheric $\delta^{13}C$ (Francey et al., 1999).
[g]Aumont et al. (2001); we assumed this flux to have the same $\delta^{13}C$ as mean terrestrial photosynthesis.

between the northern and southern mid-latitudes.) We compared this gradient with that predicted by the MATCH atmospheric transport model to result from air–sea gas exchange for different values of $\langle k \rangle$ and n. Based on the spread of TransCom models, we estimated the atmospheric transport uncertainty at ± 1.0‰, for a total uncertainty of ± 1.9‰ for the model-data comparison.

3.5. Air–sea ^{13}C exchange

We constructed an isotopic budget of ^{13}C in the atmosphere for around 1995 based on the observed rate of decline in $\delta^{13}C$ of atmospheric CO_2 together with estimates of fossil fuel emissions and terrestrial–biosphere and ocean exchanges and their isotopic composition (Table 3). We used the ocean uptake of anthropogenic CO_2 estimated on the basis of ocean DIC mea-

surements (2.2 ± 0.25 Pg C/yr for 1995) (Mikaloff Fletcher et al., 2006) to estimate the net carbon uptake of the land biosphere by difference (Table 3). This budget implies a disequilibrium air–sea ^{13}C isotope flux of 77 ± 16 Pg C ‰/yr out of the ocean for the mid-1990s (Table 3), which agrees well with the estimate of 62 ± 32 Pg C ‰/yr for a period centred in the 1980s derived by Quay et al. (2003) from observations of the decline in ocean $\delta^{13}C$ between the 1970s and 1990s. (Our simulation of ocean ^{13}C uptake suggests that the air–sea ^{13}C flux was some 14 Pg C ‰/yr larger in the mid-1990s as compared with the mid-1980s, improving the agreement between our estimate and that of Quay et al. (2003).) A steady-state 8 ± 4 Pg C ‰/yr flux into the ocean is needed to balance the influx of ~0.4 Pg C/yr of organic material depleted by ~19‰ relative to the atmosphere that enters as runoff (Heimann and

Maier-Reimer, 1996; Aumont et al., 2001) (Table 3). Adding this to the disequilibrium flux, we arrive at a total air–sea ^{13}C flux of 70 ± 17 Pg C ‰/yr. We compared this value with the flux predicted by estimates of the air–sea δ^{13}C disequilibrium based on surface ocean measurements, combined with different formulations for air–sea gas transfer.

Extensive, accurate measurements of the δ^{13}C of sea-surface DIC were made for the first time in the 1980s and 1990s as part of WOCE and related cruises (Gruber et al., 1999; Quay et al., 2003). We interpolated the sea-surface δ^{13}C measurements in GLODAP (mostly taken 1991–1999; median year, 1995) and used latitudinally and seasonally varying values for the δ^{13}C of atmospheric CO_2 for the mid 1990s based on measurements from the Scripps (Keeling et al., 1995) and NOAA/CMDL (Trolier et al., 1996) networks together with isotopic fractionation factors for air–sea exchange from Zhang et al. (1995) to predict the ^{13}C isotope flux for different global mean air–sea gas transfer velocities $\langle k \rangle$ and exponential dependences on wind speed n.

In comparing this predicted isotope flux with that inferred from the atmospheric record, additional uncertainties are introduced by possible error in the fractionation factors, by the interpolation of sea-surface δ^{13}C, and by any intercalibration offset between the atmospheric and sea-surface δ^{13}C measurements. As a sensitivity test, we tried using the sea-surface δ^{13}C field of Gruber and Keeling (2001), which is based on different measurements and interpolation procedures, and found that the predicted global air–sea isotope flux was within about 5 Pg C ‰/yr of that obtained by interpolating δ^{13}C measurements from GLODAP, suggesting that interpolation and calibration errors in the δ^{13}C fields are probably smaller than the uncertainty in inferring the air–sea ^{13}C flux from atmospheric and other observations, which we estimated at ± 17 Pg C ‰/yr (Table 3).

The latitudinal contrast in the direction of the ^{13}C isotope flux would have also existed in pre-industrial times, and we can assume that, since the δ^{13}C of atmospheric CO_2 changed much more slowly, the net air–sea isotope flux was small. Specifically, at steady state, we would expect an air–sea flux of 8 ± 4 Pg C ‰/yr into the ocean, to balance incoming river carbon (Table 3). The pre-industrial sea-surface δ^{13}C can be estimated from the WOCE-era distribution by subtracting from it the impact of recent exchange with atmospheric CO_2, whose δ^{13}C has been declining due to fossil emissions. We used a simulation with MOM ocean transport model fields (Primeau, 2005), with the OCMIP air–sea gas exchange parametrization and a history of the decline in the δ^{13}C of atmospheric CO_2 since 1800 reconstructed from gas trapped in ice (Francey et al., 1999), to estimate this perturbation in sea-surface δ^{13}C. To allow for error in the estimated perturbation, we increased the assumed uncertainty of the pre-industrial flux to ± 10 Pg C ‰/yr for the purpose of comparing it with the predicted flux under different air–sea gas exchange scenarios.

4. Results: ocean bomb ^{14}C

4.1. Total amount of ocean bomb ^{14}C

The total ocean bomb ^{14}C uptake simulated using our ocean model depends primarily on the global mean transfer velocity $\langle k \rangle$ (Fig. 5). Increasing $\langle k \rangle$ by 1% increases the simulated GEOSECS-era inventory by around 0.7% and the WOCE-era inventory by around 0.5%. Especially for the later (WOCE) period, modelled uptake is also slightly greater at high n, since this shifts uptake to high latitudes, where more deep water reaches the surface over a given period than at low latitudes so that the exchange-weighted air–sea disequilibrium term ($\Delta^{14}_{sea}C - \Delta^{14}_{air}C$) in eq. (4) is more negative.

When $\langle k \rangle$ is equal to the Wanninkhof (1992) value of 20.6 cm/hr, our model ocean total is 280–290×10^{26} atoms for the beginning of 1975 and 359–390×10^{26} atoms for mid-1994, depending on n (Fig. 5). These amounts are consistent with previous data-based estimates (Broecker et al., 1995; Key et al., 2004; Peacock, 2004). On the grid we used, the GLODAP mapping of WOCE observations (mostly using potential alkalinity to separate the bomb component) sums to 322×10^{26} atoms of bomb ^{14}C (3% higher than the 313×10^{26} atoms reported by Key et al. (2004)). This mapping excludes the Arctic Ocean and some marginal seas. Using our model concentration field for 1994 to extrapolate to the entire ocean adds an additional 11% for a WOCE-era total ocean amount of 358×10^{26} atoms (shown in Fig. 5b). Key et al. (2004) estimate the uncertainty on the total amount at 15%, or $\pm 55 \times 10^{26}$ atoms. With this uncertainty, the WOCE inventory implies a value of $\langle k \rangle$ in the range of 14–27 cm/hr (Fig. 5b). This broad range is compatible with either the Broecker et al. (1995) estimate of $305 \pm 30 \times 10^{26}$ atoms or the Peacock (2004) estimate of some $270 \pm 25 \times 10^{26}$ atoms for the global GEOSECS-era ocean total, which imply values of $\langle k \rangle$ in the range of 19–26 or 17–22 cm/hr, respectively (Fig. 5a).

The correlation between the bomb ^{14}C levels inferred from GLODAP ocean measurements and the modelled levels at the same time and space when $\langle k \rangle$ and n were close to the Wanninkhof (1992) values was $+0.93$, using either the potential alkalinity or the silica method to estimate the bomb ^{14}C component of the GLODAP observations. (This is slightly higher than the corresponding correlation of even the full model transport fields with CFC measurements, possibly because the slow air–sea exchange of ^{14}C as compared with CFCs reduces the impact of short-term variability in transport not represented in the model (e.g. Peacock et al., 2005).) At the Wanninkhof (1992) reference global mean gas transfer velocity $\langle k \rangle$ (20.6 cm/hr), our model reproduced fairly well the latitudinal structure estimated from measurements both for the GEOSECS period (Broecker et al., 1995; Peacock, 2004) and for the WOCE period (Key et al., 2004). The amount of bomb ^{14}C in the Southern Ocean was better simulated if we assumed a linear or no dependence of the transfer velocity on wind speed (Fig. 6). A caveat is that the Key
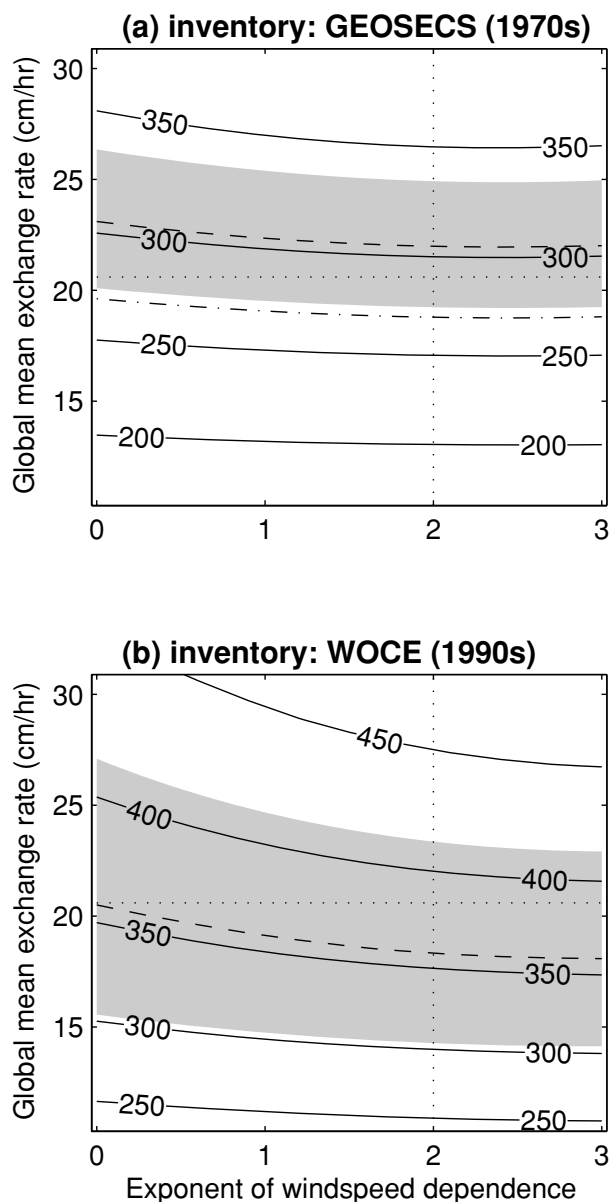
(a) inventory: GEOSECS (1970s)

(b) inventory: WOCE (1990s)

Exponent of windspeed dependence

Fig. 5. Our model-predicted total ocean bomb ^{14}C amount, in 10^{26} atoms, at the middle of the (a) GEOSECS and (b) WOCE measurement programs (1975.0 and 1994.5, respectively), when the model is run with air–sea gas exchange following eq. (4) with different values of the wind speed dependence exponent n and the global mean rate $\langle k \rangle$. Corresponding observation-based amounts from Broecker et al. (1995) [$305 \pm 30 \times 10^{26}$ atoms; dashed line and shading in (a)], Peacock (2004) [$270 \pm 25 \times 10^{26}$ atoms; dot-dashed line in (a)], and Key et al. (2004) [$358 \pm 55 \times 10^{26}$ atoms; dashed line and shading in (b)] are also shown. The dotted lines show the values for these parameters used in OCMIP (Wanninkhof, 1992).

et al. (2004) WOCE-period inventory is in part based on 1980s measurements, introducing some additional error in comparing it with model simulations of the mid-WOCE (ca. 1994) period.

While the global total is relatively insensitive to the wind speed dependence n of the gas transfer velocity, Fig. 6 suggests that the simulated latitudinal distribution of bomb ^{14}C is sensitive to n. The following approaches exploit observations of the regional distribution of bomb ^{14}C to estimate concurrently both $\langle k \rangle$ and n.

4.2. Global parametrization of gas exchange as a function of wind speed

Figure 7 shows the optimum values of the global mean gas transfer velocity $\langle k \rangle$ and the wind speed dependence exponent n (eq. 3) obtained by minimizing the misfit of modelled with measured bomb ^{14}C. Fig. 7a shows the optimum values for $\langle k \rangle$ and n estimated by fitting individual ocean GEOSECS (1970s) bomb ^{14}C measurements or their column integrals; Fig. 7b show the corresponding results when 1980s–1990s (mostly WOCE) data were used. In each panel, the letter A and the contour lines show the minimum misfit obtained using the individual measurements and the GLODAP bomb component estimate (based on potential alkalinity); B shows the minimum misfit for individual measurements and a bomb component estimate based on silica; and C and D show the minimum misfit obtained using column integrals and, respectively, potential alkalinity or silica-based estimates of the bomb component. The mean and standard deviation of the optimum parameter values for the four cases is $\langle k \rangle = 21.4 \pm 3.0$ cm/hr, $n = 0.17 \pm 0.21$ using 1970s (GEOSECS) data, and $\langle k \rangle = 18.4 \pm 1.7$ cm/hr, $n = 0.82 \pm 0.20$ using 1980s–1990s (WOCE) data. The posterior uncertainties, assuming that the each measurement is independent, were small—for example, about 0.25 cm/hr for $\langle k \rangle$ and 0.06 for n when using individual GEOSECS measurements—compared with the variability in the misfit minimum location between the cases. Model transport and other errors are likely to be highly correlated between individual measurements, so that our assumption of uncorrelated errors underestimates the actual error (overestimates the effective number of data degrees of freedom). The tendency for the optimum value of $\langle k \rangle$ to be higher when fitting against the GEOSECS period than when fitting against the WOCE period also suggests a contribution of the model transport error.

Across both periods, we found the best-fit wind speed dependence of the gas transfer velocity to be consistently less than quadratic, with the exponent n ranging from below zero (which would mean that regions with low mean wind speed tend to have high gas transfer velocities) to about 1, while $\langle k \rangle$ ranged from 16 to 23 cm/hr. Taking the mean and standard deviation of the minimum-misfit $\langle k \rangle$ and n values across all eight cases shown in Fig. 7 (first setting any negative values for the optimum n to 0), we obtained $n = 0.5 \pm 0.4$ and $\langle k \rangle = 20 \pm 3$ cm/hr. We take this to be our best estimate of the parameters in a power-law
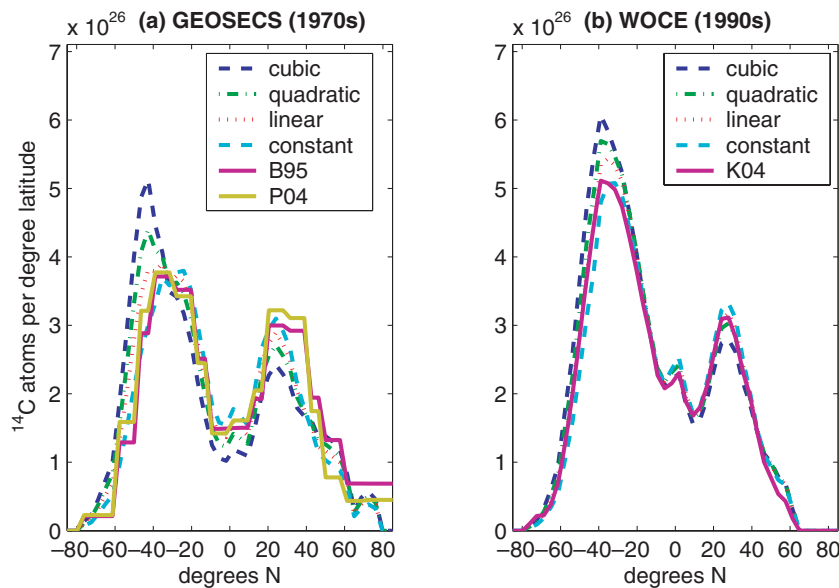
Fig. 6. Modelled latitudinal distribution of bomb ^{14}C in the ocean, for a global mean gas transfer velocity $\langle k \rangle$ of 20.6 cm/hr and a dependence on wind speed ranging from cubic to none ($n = 3, 2, 1$ or 0). A lower dependence on wind speed leads to relatively less uptake at the mid-latitudes and more near the equator. In panel (a), the 1975.0 modelled distribution is compared with extrapolations from GEOSECS observations in $10°$ bands by Broecker et al. (1995) and by Peacock (2004) (mean of her CFC- and anthropogenic CO_2-based extrapolation approaches). In panel (b), the 1994.5 modelled distribution is compared to the GLODAP gridded distribution based on WOCE observations (Key et al., 2004); the modelled distribution is summed only over the grid cells for which the gridded distribution is available, excluding, for example, the Arctic Ocean.

relationship of gas transfer velocity with wind speed (eq. 3) that most closely reproduce the observed ocean distribution of bomb ^{14}C.

4.3. Estimates of the mean gas transfer velocity by region

Figure 8 shows the regional mean gas transfer velocities estimated from GEOSECS and from WOCE ocean ^{14}C measurements, compared with the values implied by the Wanninkhof (1992) parametrization. Figure 9 compares these estimated regional rates (now averaging the estimates from GEOSECS and from WOCE) with those predicted using commonly-used published parametrizations of the gas transfer velocity as a function of wind speed, shown as solid curves. The gas transfer velocities we estimated are somewhat higher than that implied by the Wanninkhof (1992) parametrization in the north subtropical Atlantic, in the south Pacific and in the Equatorial Pacific and Atlantic, and lower in the northernmost Atlantic and in the Southern Ocean, where wind speeds are greatest. Overall, only a weak relationship with regional wind speed is evident (Fig. 9). Specifically, the best-fit power-law relationship between regional root-mean-square wind speed and the estimated regional transfer velocities—derived by minimizing the 1-norm misfit, with the uncertainty for each of the estimated transfer velocities taken to be the between-case standard deviations (shown in Fig. 9 as grey vertical bars)—has an exponent n of 0.61 ± 0.65 and a global mean $\langle k \rangle$ of 19.2 ± 0.6 cm/hr (black dashed curve in Fig. 9). This relationship implies typically higher gas transfer velocities at low wind speeds and lower rates at high wind speeds than the Wanninkhof (1992) quadratic or Wanninkhof and McGillis

(1999) cubic dependence, but an only slightly lower global mean transfer velocity, and generally higher transfer velocities compared with the Liss and Merlivat (1986) relationship, which assumes a lower global mean transfer velocity (Fig. 9). These values are consistent with the parameter values estimated in the previous section from a global fit to eq. (3). The regional transfer velocities estimated from the GEOSECS and the WOCE observations agree fairly well with one another (Fig. 8) and lead to similar power laws: $\langle k \rangle = 19.3 \pm 0.5$ cm/hr and $n = 0.37 \pm 0.51$ using just GEOSECS observations, and $\langle k \rangle = 18.8 \pm 1.3$ cm/hr and $n = 0.63 \pm 0.66$ using just WOCE-period observations.

4.4. Sensitivity tests

Studies using formulations of the gas transfer velocity similar to eq. 3 have found that the gas transfer velocity distribution obtained can differ somewhat depending on the wind climatology used (e.g. Wanninkhof et al., 2004; Olsen et al., 2005). As a test of the sensitivity of the estimated values of $\langle k \rangle$ and n to the wind speed distribution, we repeated our simulations of bomb ^{14}C uptake using monthly wind climatologies based on two other ocean wind speed products: (1) European Centre for Medium-Range Weather Forecasts (ECMWF) 6-hr ERA-40 reanalysis winds for 1958–1997 (http://data.ecmwf.int/data/d/era40_daily/; Kållberg et al., 2004), and (2) QuickScat satellite-measured wind stress for July 1999 to March 2006 (http://podaac.jpl.nasa.gov/products/product183.html) converted to wind speed using the Tang and Liu algorithm (Tang and Liu, 1996). The root-mean-square wind speed over the ice-free ocean was 7.61 m s^{-1} for the ECMWF climatology and 8.41 m s^{-1} for the QuickScat climatology, compared with

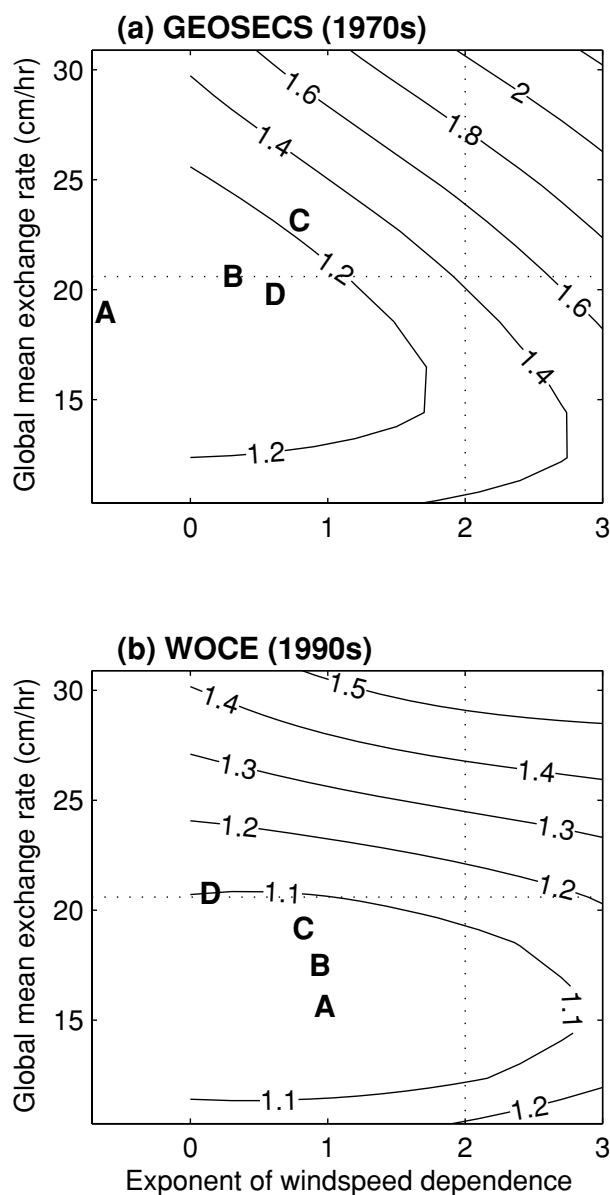## (a) GEOSECS (1970s)

(b) WOCE (1990s)

Fig. 7. Minimizing the misfit of predicted versus observed gas exchange as a function of the air–sea gas transfer velocity wind speed dependence exponent n and the global mean rate $\langle k \rangle$. (a) Misfit with GEOSECS (1970s) bomb ^{14}C observations and (b) misfit with WOCE (mostly 1990s) observations. The letters show the minimum-misfit point for different considered. The cases are: fit against individual measurements using either potential alkalinity (A) or silica (B) to estimate the background Δ^{14}C; or fit against column amount computed from measured vertical profiles, again using potential alkalinity (C) or silica (D). The contour lines show the misfit function values, relative to their minima, for the case marked (A). The dotted lines show the Wanninkhof (1992) values for the global mean gas transfer velocity and for the wind speed dependence exponent.
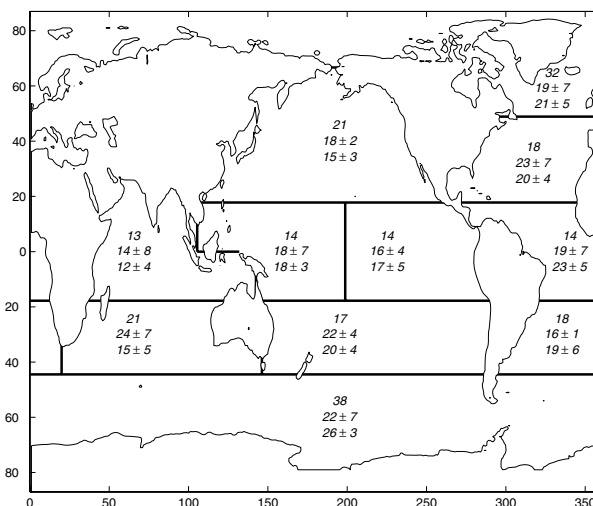

Fig. 8. Mean air–sea gas transfer velocities over 11 regions (cm/hr), derived using the quadratic relationship with wind speed of Wanninkhof (1992) and Dutay et al. (2002) (top row in each region) and estimated by optimizing the fit to the 1970s (second row) or the 1980s–1990s (third row) ocean bomb ^{14}C observations. In the second and third rows, we show the mean and the standard deviation of optimized fits obtained from four variant optimizations that featured fitting integrated vertical profile amounts instead of individual measurements and/or using silicate instead of potential alkalinity or silicate measurements to help determine the bomb component. This range gives a better idea of the actual uncertainty in our results than the uncertainty obtained by assuming error in the measurements to be uncorrelated, which is typically 1–2 cm/hr.

7.82 m s^{-1} for the SSM/I climatology. These products allowed us to calculate moments u^n other then the mean-square u^2, providing a check on the potential impact of our use of powers of the root-mean-square wind speed for all moments u^n in eq. (3).

We had available a different set of regional pulse response functions from MITgcm, which were obtained by deconvolving tracer Green's functions computed for a study of ocean anthropogenic CO_2 uptake (Mikaloff Fletcher et al., 2006). These Green's functions had a spatial structure patterned after a climatology of sea-surface pCO_2 (Takahashi et al., 2002). Given the known imposed flux history, we transformed these Green's functions to obtain pulse-response functions describing yearly mean concentration patterns resulting from an instantaneous unit pulse of a tracer into each of the 30 surface basis regions. As a test of the dependence of our results on model transport, we repeated our analysis using this set of pulse response functions and present key results as a test of the sensitivity of our gas transfer velocity optimization to the pulse response substitute model used. We also conducted simulations of bomb ^{14}C uptake with monthly-mean transport fields obtained from another ocean general circulation model, a version of the Modular Ocean Model (MOM) (Pacanowski et al., 1993) configured as described by Primeau (2005).
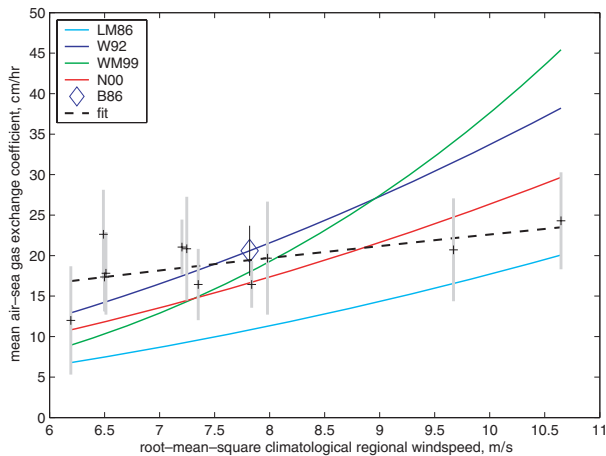
Fig. 9. Regional air–sea gas transfer velocity estimated from optimizing the fit to ocean bomb ^{14}C measurements plotted against regional root mean square wind speed (crosses show the mean of eight different optimization cases, with grey bars indicating the standard deviation among cases). Selected published formulations of air–sea gas exchange as a function of wind speed are shown for comparison: the piecewise linear relationship from Liss and Merlivat (1986), here approximated as quadratic, following Wanninkhof (1992); the quadratic relationship of Wanninkhof (1992); the cubic relationship of Wanninkhof and McGillis (1999); and the polynomial (quadratic and linear terms) relationship of Nightingale et al. (2000). To graph these formulations, we calculated first and third moments of the wind speed distribution from the mean-square (second moment) climatology assuming that wind speeds in each region followed a Rayleigh distribution. The diamond and error bar show, at the global root-mean-square wind speed, the global gas transfer velocity estimated from ocean ^{14}C evidence by Broecker et al. (1986). The best-fit power-law relationship to the regional wind speed is also drawn (dashed curve): it has an exponent of 0.61 ± 0.65 and a global mean of 19.2 ± 0.6 cm/hr.

For an assessment of how sensitive our results are to the choice of wind field and of transport model, we thus repeated our global and regional optimizations of $\langle k \rangle$ and n (as described in Sections 4.2 and 4.3 for our standard case) for four variant cases: (a) using the ECMWF wind climatology; (b) using the QuickScat wind climatology; (c) using deconvolved pulse functions from the MITgcm anthropogenic CO_2 simulation as our transport model and (d) using MOM as our transport model. Table 4 summarizes our findings. Changing the wind climatology (cases a and b) resulted in only small changes in the optimum parameter values and estimated ^{14}C inventories. The MITgcm pulse functions from the anthropogenic CO_2 simulation (case c) also yield similar parameter values but show a slightly different ^{14}C uptake history, with a higher inventory in the 1970s and a smaller proportional increase by the 1990s; the behaviour of the full MITgcm is closer to that of our 'standard' pulse functions (Fig. 4b). The MOM model yielded higher inventories in the 1970s and especially the 1990s, and a low optimum value of n (essentially zero). This

appears to be primarily due to this model's high overturning rate in the Southern Ocean, which increases the modelled bomb ^{14}C flux into the Southern Ocean and forces a low value of n (low gas transfer velocity in the Southern Ocean) to match the relatively low observed bomb ^{14}C in the Southern Ocean. This excessive tracer uptake in the Southern Ocean in this model is also seen in modelled CFC-11 uptake (not shown). By contrast, the good match between observations and MITgcm-modelled CFC-11 in the Southern Ocean (Fig. 4a) suggests that modelled Southern Ocean downward mixing in MITgcm is not excessive. The difference between the two models illustrates how air–sea gas transfer velocities inferred by comparing observed with modelled ocean tracer concentrations can be affected by bias in model transport.

While the transport model and wind field choice thus introduce some variability, a value of $\langle k \rangle$ in the 20 ± 3 cm/hr range and a low value of n seem to be robustly inferred from ocean bomb ^{14}C measurements. We turn to other carbon-14 and carbon-13 observations to determine whether our results are consistent with those as well—in particular, whether our finding that $n < 2$ holds up.

5. Results: other ^{14}C observations

5.1. 1990s air–sea ^{14}C exchange

Our fit for the dependence of the gas transfer velocity on wind speed to ocean bomb ^{14}C observations (taking $\langle k \rangle = 20$ cm/hr and $n = 0.5$) yielded a predicted atmospheric Δ^{14}C decline rate of 6.9‰/yr, while the predicted decline rate was 8.7‰/yr assuming the Wanninkhof (1992) quadratic dependence on wind speed, and 9.7‰/yr assuming the cubic dependence of Wanninkhof and McGillis (1999) (Fig. 10a). The observed decline rate together with our estimate of the combined measurement uncertainty and uncertainties in the other influences (Table 1) of 7.0 ± 1.4‰/yr is compatible with only some $(\langle k \rangle, n)$ pairs of parameter values. For example, if we assume that $\langle k \rangle$ is 20 cm/hr, then the observed decline rate suggests that n is around 0.6. The $1-\sigma$ range given the estimated uncertainty of 1.4‰ is 0–2.0, meaning that a cubic dependence on wind speed would lead to too fast a decline in atmospheric Δ^{14}C. If we assume that $n = 0.5$, $\langle k \rangle$ is 20 ± 4 cm/hr.

At the Wanninkhof (1992) value for $\langle k \rangle$, the predicted Venezuela-Southern Ocean gradient was 2.6‰ for our parametrization of the dependence of the gas transfer velocity on wind speed, 7.5‰ assuming a quadratic dependence, and 10.8‰ assuming a cubic dependence (Fig. 10b). The measured gradient of 5.6 ± 4.5‰, suggests that n is around 1.5 (range: 0–2.9), if we assume that $\langle k \rangle$ is 20 cm/hr. If we assume that $n = 0.5$, the latitudinal gradient suggests that $\langle k \rangle$ is 28 ± 13 cm/hr.

In our simulations using an atmospheric model, the wind speed dependence of the gas exchange transfer velocity was predicted

Table 4. Sensitivity tests of the dependence of the fit of the air–sea gas transfer velocities to ocean bomb ^{14}C data on wind speed climatology and transport model

Designation	Wind	Transport	Globally optimum parameter values		Bomb ^{14}C inventory $(10^{26}$ atoms)[a]		Fit to regional gas transfer velocities	
			$\langle k \rangle$ (cm/hr)	n	1975.0	1994.5	$\langle k \rangle$ (cm/hr)	n
Standard	SSM/I	MITgcm uniform pulses	20 ± 3	0.5 ± 0.4	276 ± 29	360 ± 28	19 ± 1	0.6 ± 0.7
(a)	ECMWF	MITgcm uniform pulses	20 ± 3	0.6 ± 0.5	274 ± 27	357 ± 26	19 ± 1	0.4 ± 0.4
(b)	QuickScat	MITgcm uniform pulses	20 ± 3	0.7 ± 0.5	275 ± 28	359 ± 27	19 ± 1	0.6 ± 0.4
(c)	SSM/I	MITgcm CO_2-simulation pulses	19 ± 2	0.6 ± 0.4	293 ± 28	359 ± 23	19 ± 1	0.7 ± 0.2
(d)	SSM/I	MOM	22 ± 3	0.1 ± 0.1	304 ± 27	409 ± 28	20 ± 1	-0.2 ± 0.3

[a]As simulated under the globally optimum parameter values for each case—the uncertainty given includes only the effect of the uncertainty in the parameter values.

to have a dominant effect on the latitudinal variation in atmospheric $\Delta^{14}C$ in the southern hemisphere (Fig. 11). Accurate measurements and models may be able to use this latitudinal variation to determine the mean transfer velocity in the Southern Ocean independently of ocean-interior ^{14}C.

5.2. *Pre-industrial air–sea ^{14}C exchange*

The dependence of the ocean uptake estimated from the sea-surface $\Delta^{14}C$ distribution on n was weak: the predicted air–sea flux was 4.9 kg ^{14}C/yr for our parametrization for the dependence of the gas transfer velocity on wind speed ($n = 0.5$), 5.8 assuming a quadratic dependence ($n = 2$, as in Wanninkhof (1992)), and 6.2 assuming a cubic dependence ($n = 3$, as in Wanninkhof and McGillis (1999)). These are all within the estimated uncertainty in pre-industrial ^{14}C flows in the oceans. Conversely, as long recognized (Craig, 1957; Broecker and Peng, 1982), the pre-industrial ^{14}C steady state does fix the global mean transfer velocity $\langle k \rangle$ to within ~25%, supporting the range we and earlier workers derived from ocean bomb ^{14}C measurements. Specifically, if we assume that the wind speed dependence exponent n is 0.5, $\langle k \rangle$ must be 22 ± 4 cm/hr for the air–sea flux to have been in the range of 5.4 ± 1 kg/yr.

We also compared the observed pre-industrial Britain-New Zealand gradient in atmospheric $\Delta^{14}C$ of 4.8 ± 1.6‰ with that predicted by our atmospheric transport model for different values of $\langle k \rangle$ and n (Fig. 10d). The predicted gradient was 3.7‰ for our parametrization of the dependence of the gas transfer velocity on wind speed, 5.9‰ assuming the Wanninkhof (1992) quadratic dependence, and 7.2‰ assuming the Wanninkhof and McGillis (1999) cubic dependence. If we assume a global mean velocity $\langle k \rangle$ of 20 cm/hr, the observed gradient of 4.8‰ suggests that n is around 1.3 (range: 0–2.7); if we assume that the wind speed dependence exponent n is 0.5, the observed gradient suggests that $\langle k \rangle$ is 25 ± 10 cm/hr.

6. Results: The air–sea ^{13}C isotope flux

The contemporary air–sea ^{13}C isotope flux only weakly constraints the mean gas transfer velocity (Fig. 12a). However, it provides strong support for a low wind speed exponent. The predicted 1990s air-sea isotope flux was 61 Pg C ‰/yr for our gas exchange parametrization, 37 Pg C ‰/yr for the Wanninkhof (1992) quadratic dependence on wind speed, and 19 Pg C ‰/yr for the Wanninkhof and McGillis (1999) cubic dependence. Comparing the predicted isotope fluxes with that estimated from the atmospheric ^{13}C budget (Table 3) suggested that the wind speed dependence exponent n is low (Fig. 12a). If $\langle k \rangle = 20$ cm/hr, n must be less than 1.1 to result in the isotope flux of 70 ± 17 Pg C ‰/yr inferred from observations.

In the reconstructed pre-industrial case, a steady state assumption also implied a relatively low dependence on wind speed (Fig. 12b). The predicted fluxes (with the negative sign denoting an isotope flux of ^{13}C into the ocean) were 0 Pg C ‰/yr for our gas exchange parametrization, -19 Pg C ‰/yr for the Wanninkhof (1992) quadratic dependence on wind speed, and -34 Pg C ‰/yr for the Wanninkhof and McGillis (1999) cubic dependence. Again, if $\langle k \rangle = 20$ cm/hr, n must be around 1.2 (range: 0.3–1.9) for the isotope flux to be within the range of -8 ± 10 Pg C ‰/yr implied under a steady-state assumption.

7. Discussion

7.1. *The air–sea gas transfer velocity: comparison with previous results*

Our comparison of modelled with measured ocean bomb ^{14}C distributions, whether we solve for a best-fit power-law relationship with wind speed or solve for mean transfer velocity by region, suggests that globally, mean gas exchange rates increases only about linearly with root-mean-square climatological
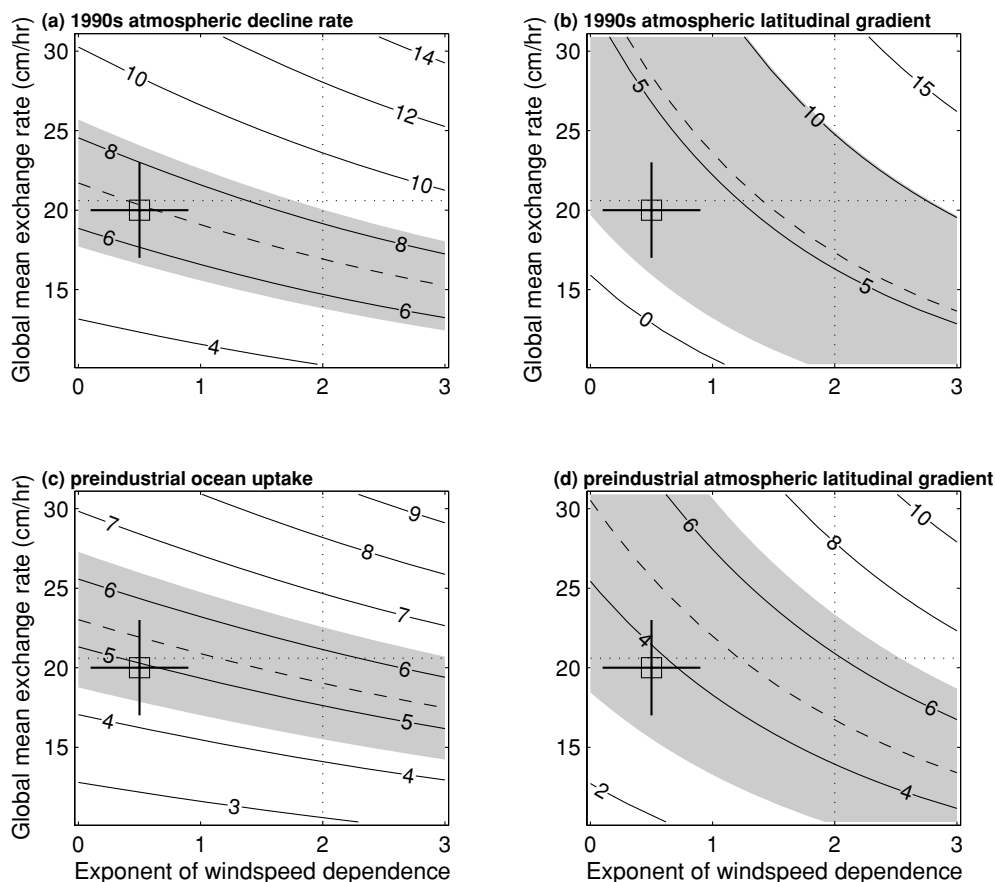
Fig. 10. Effect of the air–sea gas exchange parametrization on predicted total ocean ^{14}C uptake and on latitudinal gradients in atmospheric Δ^{14}C. The dotted lines show the Wanninkhof (1992) values for the global mean gas transfer velocity and for the wind speed dependence exponent. The square and error bars mark the parameter values that we found to best-fit ocean bomb ^{14}C measurements. The dashed lines show the approximate uptake or latitudinal gradients inferred from observations, and the shading shows the 1 standard deviation uncertainty range both by measurement error and by error in other components of the measured-modelled comparison, such as atmospheric transport. (a) Decline rate (in ‰/yr) of atmospheric Δ^{14}C around 1994, based on sea-surface Δ^{14}C interpolated from WOCE observations, atmospheric Δ^{14}C from atmospheric observations, and estimates of isotope fluxes due to biosphere exchange, cosmogenic ^{14}C production and fossil carbon emissions. Observations yield a decline rate of 7.0 ± 1.4 ‰/yr. (b) Latitudinal gradient in mean-annual atmospheric Δ^{14}C [Llano de Hato, Venezuela (8°N)–Macquarie Island (54°S)] around 1994, based on sea-surface Δ^{14}C interpolated from WOCE observations, atmospheric Δ^{14}C from atmospheric observations, and estimates of isotope fluxes due to biosphere exchange, cosmogenic ^{14}C production, and fossil carbon emissions, calculated with the atmospheric transport model MATCH. Observations reported by Levin and Hesshaimer (2000) yield a difference of 5.6 ± 4.5‰. (c) Steady-state ocean ^{14}C uptake (in kg/yr) assuming an estimated pre-industrial sea-surface Δ^{14}C distribution and mean atmospheric Δ^{14}C at 0‰. For comparison, 5.4 ± 1 kg/yr would be needed to replace the decay of ^{14}C in the ocean DIC pool. (d) Steady-state latitudinal atmospheric Δ^{14}C gradient (Britain–New Zealand, in each hemisphere's summer; in permil) calculated with the atmospheric transport model MATCH, assuming an estimated pre-industrial sea-surface Δ^{14}C distribution and mean atmospheric Δ^{14}C at 0‰. For comparison, pre-industrial tree-ring measurements reported by Hogg et al. (2002) yield a difference of 4.8 ± 1.6 ‰.

wind speed ($n = 0.5 \pm 0.4$), and that latitudinal gradients in the gas transfer velocity are smaller than a quadratic or, especially, a cubic dependence on wind speed would imply. The requirement of an approximate pre-industrial steady state constrains the global mean transfer velocity $\langle k \rangle$ (Fig. 10c), and yields values that cover the range we obtained from ocean bomb ^{14}C data. The pre-industrial latitudinal gradient, as well as 1990s ocean surface and atmospheric measurements, are also sensitive to the wind speed dependence exponent n (Figs. 10a, b and d), although

measurement and other uncertainties meant that some of the data we considered are consistent with a wide range of parameter values. The observed decline rate of atmospheric Δ^{14}C (Fig. 10), as well as the requirement that the air–sea ^{13}C isotope flux estimated from sea-surface δ^{13}C measurements be consistent with the recent atmospheric δ^{13}C history and with an approximate pre-industrial steady-state (Fig. 12), constrain n to be less than 2, which agrees with the range we estimate from ocean bomb ^{14}C data. Table 5 lists the values for $\langle k \rangle$ and n estimated from

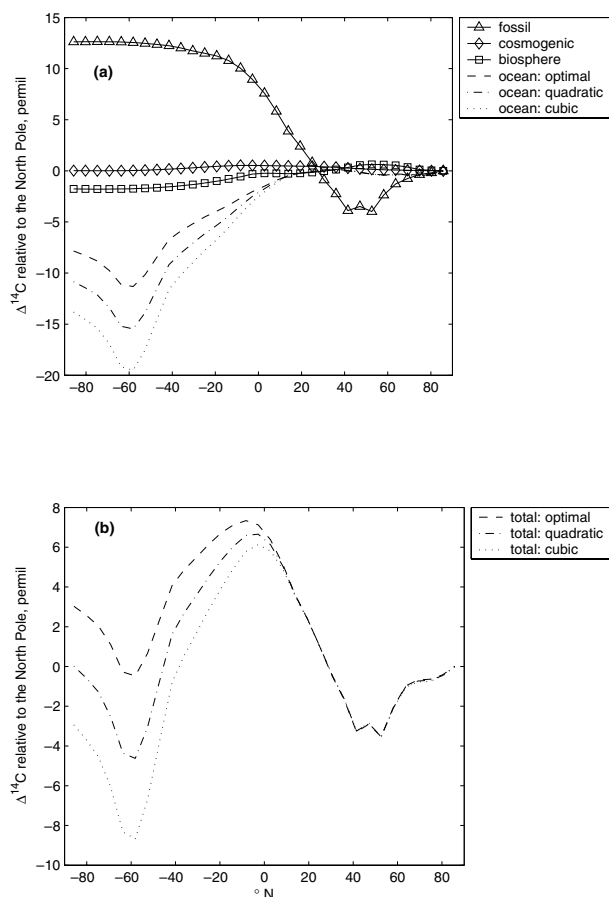*Fig. 11.* Predicted mean latitudinal gradient in $\Delta^{14}C$ of atmospheric CO_2 around 1994, taking into account the primary processes likely to cause spatial heterogeneities. We show the effect of modelled ocean uptake using measured sea-surface $\Delta^{14}C$ (Key et al., 2004) and either our optimized parametrization of the increase of the gas transfer velocity with wind speed (close to linear, with an exponent $n = 0.5$) or quadratic or cubic parametrizations ($n = 2$ or 3). (a) Modelled contribution by process. Fossil fuel emissions, concentrated in the northern mid-latitudes, dilute atmospheric ^{14}C, while respired CO_2 from the land biosphere contains high levels of bomb ^{14}C and leads to a smaller enhancement in $\Delta^{14}C$ over tropical forests and the northern mid-latitudes. Exchange with ^{14}C-depleted carbon in the Southern Ocean reduces atmospheric $\Delta^{14}C$ in the southern mid-latitudes, with the modelled magnitude of the depletion depending on the assumed dependence of the air–sea gas transfer velocity on wind speed. (b) Resultant modelled gradient. While the $\Delta^{14}C$ distribution in the northern hemisphere is unaffected by the assumed form of the air–sea gas transfer velocity, this form has a major influence on the $\Delta^{14}C$ distribution in the southern hemisphere.

the various approaches we have presented. Our estimate of the global mean air–sea gas transfer velocity for ice-free water at a Schmidt number of 660—20 ± 3 cm/hr—matches well with earlier estimates based on ocean bomb ^{14}C (Broecker et al., 1985), natural ^{14}C (Broecker and Peng, 1982), and radon-222 (Peng et al., 1979).

If we take $\langle k \rangle = 20 \pm 3$ cm/hr and $n = 0.5 \pm 0.4$, our ocean transport simulations suggest that the total amount of bomb ^{14}C in the ocean was some $276 \pm 29 \times 10^{26}$ atoms at the beginning of 1975 (close to that of Peacock (2004) and supporting her finding that the Broecker et al. (1995) estimate is biased slightly high, although remaining within error of the latter estimate) and $360 \pm 28 \times 10^{26}$ atoms at the middle of 1994 (very similar to the estimate of Key et al. (2004) adjusted for the ocean volume excluded from their inventory). We found no indication from observations of ocean bomb or natural ^{14}C uptake that the global mean air–sea gas transfer velocity is much lower than the original estimates based on GEOSECS, as Hesshaimer et al. (1994) argue.

Some earlier studies support our result of a relatively weak latitudinal variation in the mean air–sea gas transfer velocity. These include the radon-222 profiles evaluated by Peng et al. (1979), reflecting gas transfer velocity averaged over a few days, which showed little effect of wind speed and a fairly weak latitudinal gradient, and the study of pre-industrial ^{14}C by Braziunas et al. (1995), which found it necessary to revise the mean air–sea transfer velocity in the Southern Ocean (south of 50 °S) down to $\sim$31 cm/hr to account for the relatively small north–south $\Delta^{14}C$ gradient found in tree rings. A low dependence of the gas transfer velocity on wind speed was also suggested to be most consistent with pre-industrial steady-state for the air–sea ^{13}C isotope flux in an analysis by Heimann and Monfray (1989) based on sparse GEOSECS measurements of sea-surface $\delta^{13}C$.

The formulations for quadratic or cubic dependence of gas transfer on wind speed proposed by Wanninkhof (1992) and Wanninkhof and McGillis (1999), respectively, were largely based on field studies that used tracer release experiments or eddy covariance measurements of gas fluxes to evaluate the dependence of gas exchange on wind speed, typically over a few days to weeks. Extrapolating from the results of a few measurement campaigns to a relationship with wind speed suitable for use globally introduces substantial uncertainty. Direct measurement of air–sea gas fluxes is difficult and is subject to a number of sources of potential and systematic error, despite recent technical improvements (e.g. Fairall et al., 2000). As well, the apparent dependence of gas exchange on a variety of factors not directly tied to wind speed, including surfactants, rain and wave height (Frost and Upstill-Goddard, 1999; Woolf, 2005), means that the gas transfer velocity at a given wind speed could vary considerably between places and seasons depending on these other conditions. This is particularly true for extrapolations of the transfer velocity to high wind speed, where theory and laboratory evidence suggest that the gas transfer velocity saturates under some conditions (Komori et al., 1993; Donelan et al., 2004). As an example of the influence of factors other than wind speed, McGillis et al. (2004) found that the gas transfer velocity inferred from CO_2 eddy covariance in the eastern equatorial Pacific varied little with wind speed but was strongly affected by temperature gradients in the ocean mixed layer, which promoted surface turbulence. Accurate long-term direct measurements of
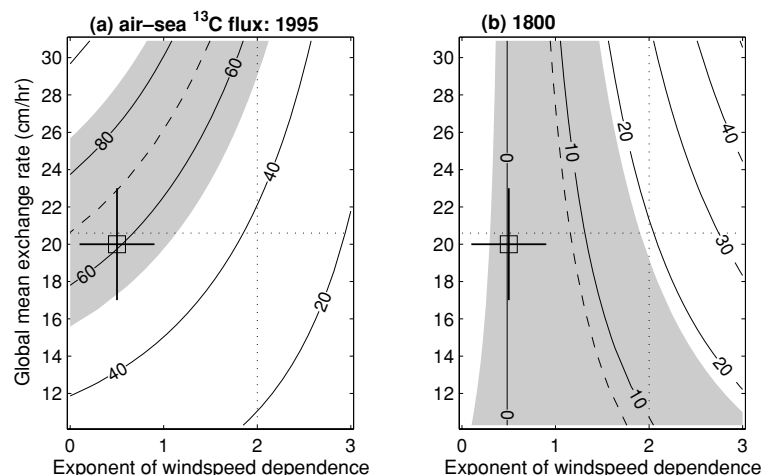
Fig. 12. Effect of the air–sea gas exchange parametrization on the ^{13}C isotope flux out of the ocean, in Pg C ‰/yr, derived from observations of sea-surface and atmosphere δ^{13}C, (a) for the mid-1990s and (b) pre-industrially. The dashed line and shading in (a) shows the observation-based estimate (± 1 standard deviation) of 70 ± 17 Pg C ‰/yr; the corresponding constraint for (b) is -8 ± 10 Pg C ‰/yr. The dotted lines show the Wanninkhof (1992) values for the global mean gas transfer velocity and for the wind speed dependence exponent. The square and error bars mark the parameter values that we found to best fit ocean bomb ^{14}C measurements.

Table 5. Summary of ^{14}C and ^{13}C constraints on the global mean air–sea gas transfer velocity $\langle k \rangle$ and its wind speed dependence exponent n

Constraint	Implied $\langle k \rangle$ (cm/hr)	Implied n
Ocean bomb ^{14}C measurements		
Ocean total amount (WOCE)	14–27	
Globally optimum fit of $\langle k \rangle$, n to measurements	20 ± 3	0.5 ± 0.4
Fit of regional gas transfer velocities	19 ± 1	0.6 ± 0.7
Other ^{14}C and ^{13}C measurements[a]		
Atmospheric Δ^{14}C: 1990s decline rate	20 ± 4	0.6 (0–2.0)
Atmospheric Δ^{14}C: 1990s latitudinal gradient	28 ± 13	1.5 (0–2.9)
Pre-industrial ocean ^{14}C uptake	22 ± 4	
Pre-industrial atmospheric Δ^{14}C latitudinal gradient	26 ± 10	1.3 (0–2.7)
Air–sea ^{13}C isotope flux, 1990s	23 ± 5	0 (0–1.1)
Air–sea ^{13}C isotope flux, pre-industrial		1.2 (0.3–1.9)

The ranges or 1-σ uncertainties given for the implied values of $\langle k \rangle$ and n are based on our estimates of measurement and model uncertainties, and/or on the spread between fits using different assumptions; see text for details.

[a]These measurements typically imply a range of compatible ($\langle k \rangle$, n) pairs (shown as the area shaded grey in Figs. 10 and 12). The implied values given here are the compatible values of $\langle k \rangle$ or n if the other parameter is set to the best-fit value determined from the ocean bomb ^{14}C distribution (i.e. n = 0.5 or $\langle k \rangle$ = 20 cm/hr), which independently constrains both parameters. We left cells blank if the measurement does not so constrain $\langle k \rangle$ or n within the range of $\langle k \rangle$ = 10–31 cm/hr and n = 0–3.

gas exchange at many representative sites would greatly improve understanding of the relative importance of different factors in governing variability in air–sea exchange across seasons and ocean regions and help suggest better parametrizations based on wind speed or other surface properties that can be determined remotely.

Our technique of deducing a parametrization of the gas transfer velocity from observations of large-scale air–sea carbon isotope exchanges implicitly averages across short-term variability in air–sea gas exchange, resulting in a parametrization that represents regional-scale gas exchange over timescales of months to decades. Our parametrization should, therefore, be appropriate for use in representing gas transfer in ocean models driven by climatological winds, but may be inappropriate for high-resolution models and for field measurements of air–sea gas

transfer, where downward tracer transport is driven by and hence covaries closely with wind-driven turbulence and other factors that may affect the gas transfer velocity. Further study is needed to assess the effect of this covariance, and whether models that include this sort of small-scale variability in upper-ocean transport should use a different dependence of gas exchange on wind speed than we found to be appropriate for climatological wind fields.

A recent review of field and laboratory measurements of the gas transfer velocity over a wide range of wind speeds (Zhao et al., 2003) found an overall power-law exponent of 1.35, only somewhat higher than our result of 0.5 ± 0.4. Zhao et al. also propose that the gas transfer velocity is better correlated with whitecap coverage than with wind speed. This would be because whitecap coverage reflects both wind speed and other
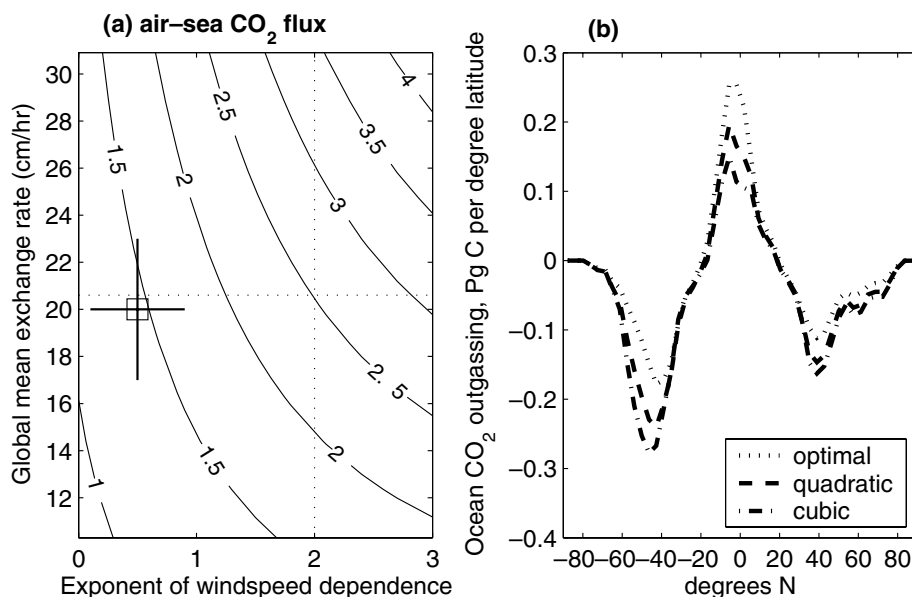
Fig. 13. Effect of the air–sea gas transfer velocity parametrization on predicted air–sea flux of CO_2, based on the air–sea pCO_2 climatology prepared by Takahashi et al. (2002) for 1995. (a) Predicted global ocean uptake of anthropogenic CO_2 (in Pg C/yr) as a function of the air–sea gas exchange parametrization. To obtain the anthropogenic CO_2 flux, we corrected the total flux by 0.7 Pg C/yr for the assumed steady-state ocean outgassing that balances an inflow of continental carbon (Aumont et al., 2001). The dashed lines show the Wanninkhof (1992) values for the global mean gas transfer velocity and for the wind speed dependence exponent. The square and error bars mark the parameter values that we found to best-fit ocean bomb ^{14}C measurements. Observational estimates of this uptake have been around 2.0–2.4 Pg C/yr. (b) Latitudinal distribution of the air–sea flux for our optimized parameter values and for parametrizations of air–sea gas exchange with quadratic or cubic dependences on wind speed.

factors that influence the gas transfer velocity, such as the presence of organic surfactant films that inhibit turbulence and the degree to which waves are fully developed at a given wind stress (which depends on the consistency of the wind direction and the distance from shore). It would be worth examining whether a parametrization based on whitecap coverage would better account for the regional variability we found in the mean gas transfer velocity, compared with a parametrization based only of wind speed. Whitecap coverage can be remotely determined using satellite instrumentation similar to that used for sensing wind speed (Monahan, 2002). Sea-surface mean-square slope is another quantity that can be sensed remotely from microwave backscatter measurements and has been suggested to predict the gas transfer velocity better than wind speed (Frew et al., 2004; Turney et al., 2005). Also, a more complex function for the dependence of the gas transfer velocity on wind speed, in which, for example, the transfer velocity levels off at low wind speeds and plateaus at high wind speeds, may well better represent the variability in the transfer velocity over a variety of time and space scales than the simple power-law relationship that we assumed.

7.2. Implications for air–sea CO_2 fluxes

We examined the effect of air–sea gas exchange parametrizations on the air–sea CO_2 flux implied by the air–sea pCO_2 difference climatology compiled by Takahashi et al. (2002) for a nominal year of 1995 (Fig. 13). The total uptake is sensitive to *n* as well as $\langle k \rangle$, since the tropical oceans, with low mean wind speeds, tend to release CO_2 while the high-latitude oceans, with higher mean wind speeds, tend to take it up. With this surface pCO_2 climatology, the predicted anthropogenic uptake is 1.4 Pg C/yr using our parametrization of the gas transfer velocity dependence on wind speed, 2.5 Pg C/yr using the Wanninkhof (1992) quadratic dependence, and 3.1 Pg C/yr assuming the Wanninkhof and McGillis (1999) cubic dependence (Fig. 13a). The uncertainty in ocean CO_2 uptake estimated using this method is large, because small adjustments to sea-surface pCO_2 due to, for example, the skin temperature correction for evaporative cooling (Van Scoy et al., 1995; Ward et al., 2004) and respiration by micro-organisms in the surface microlayer (Garabetian, 1991), as well as to errors induced by lack of sampling in some seasons and regions, have a large impact on the inferred global uptake. Independent observational estimates of anthropogenic ocean CO_2 uptake include 2.2 $\pm$ 0.25 Pg C/yr for around 1995 based on the C* method for estimating the anthropogenic enhancement of ocean DIC combined with several ocean circulation models (Mikaloff Fletcher et al., 2006), 2.0 $\pm$ 0.4 Pg C/yr for the 1990s based on water ages inferred from ocean CFC measurements (McNeil et al., 2003), and 2.4 $\pm$ 0.7 Pg C/yr for the 1990s based on atmospheric oxygen measurements (Plattner et al., 2002).

Figure 13b shows the CO_2 flux by latitude estimated from the Takahashi et al. (2002) pCO_2 climatology using our gas

transfer velocity parametrization compared with quadratic and cubic dependences on wind speed. Our lower wind speed dependence implies less CO_2 uptake in the Southern Ocean and shifts the maximum uptake there north by several degrees, which resolves part of the discrepancy between the high Southern Ocean CO_2 uptake implied by this pCO_2 climatology and a quadratic or cubic dependence of gas exchange on wind speed and the low Southern Ocean CO_2 uptake inferred from the stable atmospheric CO_2 concentrations measured over the Southern Ocean (Roy et al., 2003). The regional distribution of the ocean CO_2 uptake implied by a quadratic dependence on wind speed is used as a prior constraint in many inversions for regional CO_2 fluxes that are based on atmospheric CO_2 measurements (e.g. Gurney et al., 2003), so adopting a different dependence on wind speed could also affect the regional CO_2 sources and sinks inferred from such inversions. For example, the network of CO_2 observation stations does not distinguish land from ocean carbon sources and sinks in the tropics, so this assignment depends on the use of other information, such as the distribution of the air–sea CO_2 flux (e.g. Krakauer et al., 2004). If CO_2 outgassing from the equatorial ocean is more intense than previously assumed, a smaller tropical land source might be required to explain the observed patterns in atmospheric CO_2 concentration.

Our higher estimate for the gas transfer velocity in the eastern equatorial Pacific highlights the potential significance of pCO_2 variations there with ENSO (Feely et al., 1999, 2004b) for interannual variability in ocean CO_2 uptake. Conversely, a smaller dependence of gas exchange on wind speed makes it less likely that changes in storm frequencies are a major contributor to interannual variability in the ocean sink (Bates, 2002; Perrie et al., 2004).

7.3. *Estimating gas transfer velocities from carbon isotope distributions: limitations and directions for improvement*

Some of the data sets that we used to calculate the air–sea bomb ^{14}C flux could be refined. The zonal distribution of atmospheric $\Delta^{14}C$ in the 1960s, when gradients were very large, should be revisited in light of expanded tropical tree-ring measurements (Hua et al., 1999; Hua and Barbetti, 2004).

Judging by the differences we found between methods based on potential alkalinity and on silica for estimating the pre-bomb ocean $\Delta^{14}C$, which is used to determine the bomb ^{14}C component in post-bomb $\Delta^{14}C$ measurements, the pre-bomb $\Delta^{14}C$ distribution is a significant source of uncertainty. This is particularly important for the Southern Ocean, where because of more extensive mixing the absolute bomb $\Delta^{14}C$ enhancements tend to be smaller and thus harder to quantify, and where few early $\Delta^{14}C$ measurements were made (Broecker et al., 1960). Measurements of $\Delta^{14}C$ in banded ahermatypic corals (Goldstein et al., 2001; Frank et al., 2004), which grow in cold water, could help calibrate the pre-bomb $\Delta^{14}C$ profile in the South-

ern Ocean. Coral $\Delta^{14}C$ time-series in general provide unique chronologies of bomb ^{14}C arrival, and could supplement single measurements of water $\Delta^{14}C$ such as the ones in GLODAP as evidence for air–sea gas transfer velocity and for ocean transport processes.

Another uncertainty in our ocean bomb ^{14}C results comes from our ocean transport model. While our model appears to represent the global inventory and latitudinal distribution of tracers such as CFCs and bomb ^{14}C quite accurately over decadal timescales and its finding of relatively low latitudinal variability in air–sea gas exchange appears robust, it is harder to validate its skill in assigning uptake to smaller regions, especially given the loss of resolution imparted by using regional pulse functions. Intercomparison of the dependence of patterns of uptake of bomb ^{14}C on air–sea transfer velocity over different transport models, similar to the OCMIP-3 project of solving for best-fit air–sea CO_2 fluxes from different models (Mikaloff Fletcher et al., 2006), would at least permit better assessment of the magnitude of transport error. Ultimately, a fully inverse approach, where ocean circulation fields and the distribution of the mean air–sea gas transfer velocity are estimated simultaneously using measurements of bomb ^{14}C together with other ocean tracers (cf. Schlitzer, 2000) within an ocean data assimilation framework such as ECCO, is likely to be the most effective way to utilize the large number of available ocean $\Delta^{14}C$ measurements to infer detailed spatial patterns in gas transfer velocity.

We have shown that the 1990s rate of decline in and latitudinal profile of the $\Delta^{14}C$ of atmospheric CO_2 reflect the latitudinal distribution of the air–sea gas transfer velocity. Continued measurement of atmospheric $\Delta^{14}C$ and of sea-surface $\Delta^{14}C$ across the Southern Hemisphere would, therefore, provide information about the mean rate of air–sea gas exchange in the Southern Ocean averaged over the atmospheric transport timescale (a few months), and in principle could even detect seasonal and interannual variability in the Southern Ocean transfer velocity, although the precision requirement is high. Given the importance of Southern Ocean gas exchange to climate and to CO_2 uptake (Liss et al., 2004), a long-term measurement program should be worthwhile. To enable reasonably accurate determinations of gas exchange velocities by this method, the contribution of terrestrial biosphere respiration, stratosphere–troposphere exchange, and fossil fuel burning to the atmospheric $\Delta^{14}C$ needs to be better modelled and tested against observations such as vertical atmospheric $\Delta^{14}C$ profiles.

We have also shown that the ongoing air–sea isotopic flux of ^{13}C, as well as the pre-industrial flux, provides information about the wind speed dependence of the gas transfer velocity if the spatial distribution of the air–sea $\delta^{13}C$ disequilibrium is well known. Further work is needed to find the best way of estimating this distribution from available measurements, possibly replacing the simple interpolation that we used with a more sophisticated approach using ocean transport models to map ocean surface $\delta^{13}C$ in a way consistent with measurements, and to more fully assess

the uncertainties in $\delta^{13}C$ measurements and in the equilibrium air–sea isotopic fractionation. In particular, we neglected the seasonality of sea-surface $\delta^{13}C$, and its possible covariance with seasonal cycles in downward transport and in the gas transfer velocity, which should be assessed with coupled ocean transport and biogeochemistry modelling and with observational time series. (The same concern applies to our approaches of deriving the air–sea ^{14}C flux from pre-industrial or contemporary surface $\Delta^{14}C$ climatologies, which do not include seasonal variability.) Our pre-industrial $\delta^{13}C$ reconstruction is also of uncertain accuracy and should be verified using other transport models and, perhaps, measurements of tracers of fossil fuel CO_2 such as $C*$ (Gruber et al., 1996).

8. Conclusions

The air–sea gas transfer velocity is important for quantifying the ocean gas exchange, and both field measurements and indirect inference from tracer distributions can help in developing a consistent formulation for it. We have estimated the mean gas transfer velocity both by region and as a function of climatological monthly wind speed from ocean bomb carbon-14 measurements as well as from other carbon-14 and carbon-13 data. Although many of the approaches we used yield substantial uncertainties, our overall results support a linear or lower increase of gas transfer velocity with wind speed in the global ocean (best-fit exponent: 0.5 ± 0.4; global mean rate: 20 ± 3 cm/hr at a Schmidt number of 660).

To better characterize model transport error, we recommend either comparing carbon-14 distributions for multiple models or else solving for transport simultaneously with air–sea exchange. High-precision measurement of atmospheric carbon-14 may provide independent information on air–sea exchange, especially for the Southern Ocean.

9. Acknowledgments

References

Andres, R. J., Marland, G., Fung, I. and Matthews, E. 1996. A $1° \times 1°$ distribution of carbon dioxide emissions from fossil fuel consumption and cement manufacture, 1950-1990. *Global Biogeochem. Cycles* **10**(3), 419–429.

Asher, W., Wang, Q., Monahan, E. C. and Smith, P. M. 1998. Estimation of air-sea gas transfer velocities from apparent microwave brightness temperature. *Marine Tech. Soc. J.* **32**(2), 32–40.

Aster, R. C., Borchers, B. and Thurber, C. H. 2005. *Parameter Estimation and Inverse Problems*, p. 301, Elsevier Academic Press, Amsterdam and Boston.

Aumont, O., Orr, J. C., Monfray, P., Ludwig, W., Amiotte-Suchet, P. and co-authors. 2001. Riverine-driven interhemispheric transport of carbon. *Global Biogeochem. Cycles* **15**(2), 393–405.

Bacastow, R. B., Keeling, C. D., Lueker, T. J., Wahlen, M. and Mook, W. G. 1996. The C-13 Suess effect in the world surface oceans and its implications for oceanic uptake of CO_2: analysis of observations at Bermuda. *Global Biogeochem. Cycles* **10**(2), 335–346.

Bates, N. R. 2002. Interannual variability in the global uptake of CO_2. *Geophys. Res. Lett.* **29**(5), 1059, doi:10.1029/2001GL013571.

Battle, M., Bender, M. L., Tans, P. P., White, J. W. C., Ellis, J. T. and co-authors. 2000. Global carbon sinks and their variability inferred from atmospheric O_2 and delta ^{13}C. *Science* **287**(5462), 2467–2470.

Boutin, J. and Etcheto, J. 1996. Consistency of Geosat, SSM/I, and ERS-1 global surface wind speeds—comparison with in situ data. *J. Atmos. Ocean. Technol.* **13**(1), 183–197.

Boutin, J. and Etcheto, J. 1997. Long-term variability of the air-sea CO_2 exchange coefficient: consequences for the CO_2 fluxes in the equatorial Pacific ocean. *Global Biogeochem. Cycles* **11**(3), 453–470.

Boyer, T. P., Stephens, C., Antonov, J. I., Conkright, M. E., Locranini, R. A. and co-authors. 2002. *World Ocean Atlas 2001, Volume 2: Salinity*, p. 165, US Government Printing Office, Washington.

Braziunas, T. F., Fung, I. Y. and Stuiver, M. 1995. The preindustrial atmospheric $^{14}CO_2$ latitudinal gradient as related to exchanges among atmospheric, oceanic, and terrestrial reservoirs. *Global Biogeochem. Cycles* **9**(4), 565–584.

Broecker, W., Gerard, R., Ewing, M. and Heezen, B. C. 1960. Natural radiocarbon in the Atlantic Ocean. *J. Geophys. Res.* **65**(9), 2903–2931.

Broecker, W. S., Ledwell, J. R., Takahashi, T., Weiss, R., Merlivat, L. and co-authors. 1986. Isotopic versus micrometeorological ocean CO$_2$ fluxes - a serious conflict. *J. Geophys. Res.* **91**(C9), 517–527.

Broecker, W. S. and Peng, T.-H. 1982. *Tracers in the sea*, p. 690, Lamont-Doherty Geological Observatory, Palisades, NY.

Broecker, W. S., Peng, T. H., Ostlund, G. and Stuiver, M. 1985. The distribution of bomb radiocarbon in the ocean. *J. Geophys. Res.* **90**(C4), 6953–6970.

Broecker, W. S., Sutherland, S., Smethie, W., Peng, T. H. and Ostlund, G. 1995. Oceanic radiocarbon - Separation of the natural and bomb components. *Global Biogeochem. Cycles* **9**(2), 263–288.

Caldeira, K. and Wickett, M. E. 2003. Anthropogenic carbon and ocean pH. *Nature* **425**(6956), 365.

Caldeira, K., Rau, G. H. and Duffy, P. B. 1998. Predicted net efflux of radiocarbon from the ocean and increase in atmospheric radiocarbon content. *Geophys. Res. Lett.* **25**(20), 3811–3814.

Conway, T. J., Tans, P. P., Waterman, L. S., Thoning, K. W., Kitzis, D. R. and co-authors. 1994. Evidence for interannual variability of the carbon cycle from National Oceanic and Atmospheric Administration/Climate Monitoring and Diagnostics Laboratory Global Air Sampling Network. *J. Geophys. Res.* **99**(D11), 23 831–23 855.

Craig, H. 1957. The natural distribution of radiocarbon and the exchange time of carbon dioxide between the atmosphere and the sea. *Tellus* **9**, 1–17.

Damon, P. E. and Sternberg, R. E. 1989. Global production and decay of radiocarbon. *Radiocarbon* **31**(3), 697–703.

Donelan, M. A., Haus, B. K., Reul, N., Plant, W. J., Stiassnie, M. and co-authors. 2004. On the limiting aerodynamic roughness of the ocean in very strong winds. *Geophys. Res. Lett.* **31**(18).

Druffel, E. M. and Suess, H. E. 1983. On the radiocarbon record in banded corals: exchange parameters and net transport of ^{14}CO$_2$ between atmosphere and surface ocean. *J. Geophys. Res.-Oceans Atm.* **88**(NC2), 1271–1280.

Druffel, E. R. M. 1987. Bomb radiocarbon in the Pacific: annual and seasonal timescale variations. *J. Mar. Res.* **45**, 667–698.

Druffel, E. R. M. 1989. Decade time scale variability of ventilation in the North Atlantic: high-precision measurements of bomb radiocarbon in banded corals. *J. Geophys. Res.* **94**(C3), 3271–3285.

Druffel, E. R. M. and Griffin, S. 1995. Regional variability of surface ocean radiocarbon from southern great barrier reef corals. *Radiocarbon* **37**(2), 517–524.

Dutay, J. C., Bullister, J. L., Doney, S. C., Orr, J. C., Najjar, R. and co-authors. 2002. Evaluation of ocean model ventilation with CFC-11: comparison of 13 global ocean models. *Ocean Modelling* **4**(2), 89–120.

England, M. H., Garcon, V. and Minster, J. F. 1994. Chlorofluorocarbon uptake in a world ocean model 1. Sensitivity to the surface gas forcing. *J. Geophys. Res.* **99**(C12), 25 215–25 233.

Esbensen, S. K. and Kushnir, Y. 1981. The heat budget of the global ocean: an Atlas based on estimates from marine surface observations. Oregon State University, Corvallis, Oregon.

Fairall, C. W., Hare, J. E., Edson, J. B. and McGillis, W. 2000. Parameterization and micrometeorological measurement of air-sea gas transfer. *Boundary-Layer Meteorology* **96**(1–2), 63–105.

Fasham, M. J. R. 2003. *Ocean Biogeochemistry: The Role of the Ocean Carbon Cycle in Global Change*, pp. 297, Springer, Berlin, New York.

Feely, R. A., Wanninkhof, R., Takahashi, T. and Tans, P. 1999. Influence of El Niño on the equatorial Pacific contribution to atmospheric CO$_2$ accumulation. *Nature* **398**(6728), 597–601.

Feely, R. A., Sabine, C. L., Lee, K., Berelson, W., Kleypas, J. and co-authors. 2004a. Impact of anthropogenic CO$_2$ on the CaCO$_3$ system in the oceans. *Science* **305**(5682), 362–366.

Feely, R. A., Wanninkhof, R., McGillis, W., Carr, M. E. and Cosca, C. E. 2004b. Effects of wind speed and gas exchange parameterizations on the air-sea CO$_2$ fluxes in the equatorial Pacific Ocean. *J. Geophys. Res.* **109**(C8), C08S03, doi:10.1029/2003JC001896.

Francey, R. J., Allison, C. E., Etheridge, D. M., Trudinger, C. M., Enting, I. G. and co-authors. 1999. A 1000-year high precision record of δ^{13}C in atmospheric CO$_2$. *Tellus* **51B**, 170–193.

Francey, R. J., Allison, C. E., Trudinger, C. M., Rayner, P. J., Enting, I. G. and co-authors. 2001. The interannual variation in global atmospheric delta^{13}C and its link to net terrestrial exchange. In: *Sixth International Carbon Dioxide Conference, Extended Abstracts*, Organizing Committee of Sixth International Carbon Dioxide Conference, Sendai, Japan, pp. 43–46.

Frank, N., Paterne, M., Ayliffe, L., van Weering, T., Henriet, J. P. and co-authors. 2004. Eastern North Atlantic deep-sea corals: tracing upper intermediate water Delta C-14 during the Holocene. *Earth Planet. Sci. Lett.* **219**(3–4), 297–309.

Frew, N. M., Bock, E. J., Schimpf, U., Hara, T., Haussecker, H. and co-authors. 2004. Air-sea gas transfer: its dependence on wind stress, small-scale roughness, and surface films. *J. Geophys. Res.* **109**(C8), C08S17.

Frost, T. and Upstill-Goddard, R. C. 1999. Air-sea gas exchange into the millennium: progress and uncertainties. In: *Oceanog. Mar. Biol.* **37**, 1–45.

Garabetian, F. 1991. ^{14}C-glucose uptake and ^{14}C-CO$_2$ production in surface microlayer and surface-water samples: influence of UV and visible radiation. *Mar. Ecol. Prog. Series* **77**(1), 21–26.

Gloor, M., Gruber, N., Hughes, T. M. C. and Sarmiento, J. L. 2001. Estimating net air-sea fluxes from ocean bulk data: methodology and application to the heat cycle. *Global Biogeochem. Cycles* **15**(4), 767–782.

Gloor, M., Gruber, N., Sarmiento, J., Sabine, C. L., Feely, R. A. and co-authors. 2003. A first estimate of present and preindustrial air-sea CO$_2$ flux patterns based on ocean interior carbon measurements and models. *Geophys. Res. Lett.* **30**(1), 1010.

Goldstein, S. J., Lea, D. W., Chakraborty, S., Kashgarian, M. and Murrell, M. T. 2001. Uranium-series and radiocarbon geochronology of deep-sea corals: implications for Southern Ocean ventilation rates and the oceanic carbon cycle. *Earth Planet. Sci. Lett.* **193**(1–2), 167–182.

Goslar, T. 2001. Absolute production of radiocarbon and the long-term trend of atmospheric radiocarbon. *Radiocarbon* **43**(2B), 743–749.

Gruber, N. and Keeling, C. D. 2001. An improved estimate of the isotopic air-sea disequilibrium of CO$_2$: implications for the oceanic uptake of anthropogenic CO$_2$. *Geophys. Res. Lett.* **28**(3), 555–558.

Gruber, N., Sarmiento, J. L. and Stocker, T. F. 1996. An improved method for detecting anthropogenic CO$_2$ in the oceans. *Global Biogeochem. Cycles* **10**(4), 809–837.

Gruber, N., Keeling, C. D., Bacastow, R. B., Guenther, P. R., Lueker, T. J. and co-authors. 1999. Spatiotemporal patterns of carbon-13 in

the global surface oceans and the oceanic Suess effect. *Global Biogeochem. Cycles* **13**(2), 307–335.

Gruber, N., Gloor, M., Fan, S. M. and Sarmiento, J. L. 2001. Air-sea flux of oxygen estimated from bulk data: implications for the marine and atmospheric oxygen cycles. *Global Biogeochem. Cycles* **15**(4), 783–803.

Gurney, K. R., Law, R. M., Denning, A. S., Rayner, P. J., Baker, D. and co-authors. 2002. Towards robust regional estimates of CO_2 sources and sinks using atmospheric transport models. *Nature* **415**(6872), 626–630.

Gurney, K. R., Law, R. M., Denning, A. S., Rayner, P. J., Baker, D. and co-authors. 2003. TransCom 3 CO_2 inversion intercomparison: 1. Annual mean control results and sensitivity to transport and prior flux information. *Tellus* **55B**, 555–579.

Heimann, M. and Maier-Reimer, E. 1996. On the relations between the oceanic uptake of CO_2 and its carbon isotopes. *Global Biogeochem. Cycles* **10**(1), 89–110.

Heimann, M. and Monfray, P. 1989. Spatial and Temporal Variation of the Gas Exchange Coefficient for CO_2: 1. Data Analysis and Global Validation, pp. 29, Max-Planck-Institut für Meteorologie, Hamburg, Germany.

Hesshaimer, V., Heimann, M. and Levin, I. 1994. Radiocarbon evidence for a smaller oceanic carbon-dioxide sink than previously believed. *Nature* **370**(6486), 201–203.

Hogg, A. G., McCormac, F. G., Higham, T. F. G., Reimer, P. J., Baillie, M. G. L. and co-authors. 2002. High-precision radiocarbon measurements of contemporaneous tree-ring dated wood from the British Isles and New Zealand: AD 1850-950. *Radiocarbon* **44**(3), 633–640.

Hua, Q. and Barbetti, M. 2004. Review of tropospheric bomb ^{14}C data for carbon cycle modeling and age calibration purposes. *Raliocarbon* **46**(3), 1273–1298.

Hua, Q., Barbetti, M., Worbes, M., Head, J. and Levchenko, V. A. 1999. Review of radiocarbon data from atmospheric and tree ring samples for the period 1945–1997 AD. *Iawa J.* **20**(3), 261–283.

Ito, T., Marshall, J. and Follows, M. 2004. What controls the uptake of transient tracers in the Southern Ocean? *Global Biogeochem. Cycles* **18**(2).

Jähne, B. and Haussecker, H. 1998. Air-water gas exchange. *Annu. Rev. Fluid Mech.* **30**, 443–468.

Joos, F. 1996. An efficient and accurate representation of complex oceanic and biospheric models of anthropogenic carbon uptake. *Tellus, Series B.* **48**(3), 397–417.

Joos, F. and Bruno, M. 1998. Long-term variability of the terrestrial and oceanic carbon sinks and the budgets of the carbon isotopes C-13 and C-14. *Global Biogeochem. Cycles* **12**(2), 277–295.

Kållberg, P., Simmons, A., Uppala, S. and Fuentes, M. 2004. The ERA-40 Archive. pp. 31, European Centre for Medium Range Weather Forecasts, Shinfield Park, England.

Keeling, C. D., Bacastow, R. B., Bainbridge, A. E., Ekdahl, C. A., Guenther, P. R. and co-authors. 1976. Atmospheric carbon-dioxide variations at Mauna-Loa Observatory, Hawaii. *Tellus* **28**, 538–551.

Keeling, C. D., Whorf, T. P., Wahlen, M. and Vanderplicht, J. 1995. Interannual extremes in the rate of rise of atmospheric carbon-dioxide since 1980. *Nature* **375**(6533), 666–670.

Key, R. M., Kozyr, A., Sabine, C. L., Lee, K., Wanninkhof, R. and co-authors. 2004. A global ocean carbon climatology: results from Global

Data Analysis Project (GLODAP). *Global Biogeochem. Cycles* **18**(4), GB4031.

Key, R. M., Quay, P. D., Schlosser, P., McNichol, A. P., von Reden, K. F. and co-authors. 2002. WOCE radiocarbon IV: Pacific Ocean results; P10, P13N, P14C, P18, P19 & S4P. *Radiocarbon* **44**(1), 239–392.

Komori, S., Nagaosa, R. and Murakami, Y. 1993. Turbulence structure and mass-transfer across a sheared air-water interface in wind-driven turbulence. *J. Fluid Mech.* **249**, 161–183.

Krakauer, N. Y., Schneider, T., Randerson, J. T. and Olsen, S. C. 2004. Using generalized cross-validation to select parameters in inversions for regional carbon fluxes. *Geophys. Res. Lett.* **31**(19), doi:10.1029/2004020323.

Levin, I. and Hesshaimer, V. 2000. Radiocarbon - A unique tracer of global carbon cycle dynamics. *Radiocarbon* **42**(1), 69–80.

Levin, I. and Kromer, B. 2004. The Tropospheric $^{14}CO_2$ level in Mid-Latitudes of the Northern Hemisphere (1959–2003). *Radiocarbon* **46**(3), 1261–1272.

Levin, I., Kromer, B., Schmidt, M. and Sartorius, H. 2003. A novel approach for independent budgeting of fossil fuel CO_2 over Europe by $^{14}CO_2$ observations. *Geophys. Res. Lett.* **30**(23), art. no. 2194.

Levin, I., Kromer, B., Wagenbach, D. and Münnich, K. O. 1987. Carbon isotope measurements of atmospheric CO_2 at a coastal station in Antarctica. *Tellus* **39B**, 89–95.

Lingenfelter, R. E. 1963. Production of carbon-14 by cosmic-ray neutrons. *Reviews of Geophysics* **1**(1), 35–55.

Linick, T. W. 1980. Bomb-produced C-14 in the surface-water of the Pacific Ocean. *Radiocarbon* **22**(3), 599–606.

Liss, P. S. and Merlivat, L. 1986. Air-sea gas exchange rates: introduction and synthesis. In: *The Role of Air-Sea Exchange in Geochemical Cycling* (ed. P. Buat-Ménard), D. Reidel, Dordrecht, pp. 113–129.

Liss, P. S., Chuck, A. L., Turner, S. M. and Watson, A. J. 2004. Air-sea gas exchange in Antarctic waters. *Antarctic Sci.* **16**(4), 517–529.

Mahowald, N. M., Rasch, P. J., Eaton, B. E., Whittlestone, S. and Prinn, R. G. 1997. Transport of ^{222}radon to the remote troposphere using the Model of Atmospheric Transport and Chemistry and assimilated winds from ECMWF and the National Center for Environmental Prediction/NCAR. *J. Geophys. Res.* **102**(D23), 28 139–28 151.

Manning, M. R., Lowe, D. C., Melhuish, W. H., Sparks, R. J., Wallace, G. and co-authors. 1990. The use of radiocarbon measurements in atmospheric studies. *Radiocarbon* **32**(1), 37–58.

Marland, G., Boden, T. A. and Andres, R. J. 2005. Global, regional, and national fossil fuel CO_2 emissions. In: *Trends: A Compendium of Data on Global Change*. Carbon Dioxide Information Analysis Center, Oak Ridge National Laboratory, U.S. Department of Energy, http://cdiac.esd.ornl.gov/trends/trends.htm.

Marshall, J., Adcroft, A., Hill, C., Perelman, L. and Heisey, C. 1997. A finite-volume, incompressible Navier Stokes model for studies of the ocean on parallel computers. *J. Geophys. Res.* **102**(C3), 5753–5766.

Masiello, C. A., Druffel, E. R. M. and Bauer, J. E. 1998. Physical controls on dissolved inorganic radiocarbon variability in the California Current. *Deep-Sea Res.* **45**(4–5), 617–642.

McGillis, W. R., Edson, J. B., Hare, J. E. and Fairall, C. W. 2001. Direct covariance air-sea CO_2 fluxes. *J. Geophys. Res.* **106**(C8), 16 729–16 745.

McGillis, W. R., Edson, J. B., Zappa, C. J., Ware, J. D., McKenna, S. P. and co-authors. 2004. Air-sea CO_2 exchange in the equatorial Pacific. *J. Geophys. Res.* **109**(C8), C08S02, doi:10.1029/2003JC002256.

McNeil, B. I., Matear, R. J., Key, R. M., Bullister, J. L. and Sarmiento, J. L. 2003. Anthropogenic CO$_2$ uptake by the ocean based on the global chlorofluorocarbon data set. *Science* **299**(5604), 235–239.

Mikaloff Fletcher, S. E., Gruber, N., Jacobson, A. R., Doney, S. C., Dutkiewcz, S. and co-authors. 2006. Inverse estimates of anthropogenic CO$_2$ uptake, transport, and storage by the ocean. *Global Biogeochem. Cycles* **20**, GB2002, doi:10.1029/2005GB002530.

Monahan, E. C. 2002. Oceanic whitecaps: sea surface features detectable via satellite that are indicators of the magnitude of the air-sea gas transfer coefficient. *Proc. Indian Acad. Sci.-Earth Planet. Sci* **111**(3), 315–319.

Murnane, R. J., Sarmiento, J. L. and Le Quéré, C. 1999. Spatial distribution of air-sea CO$_2$ fluxes and the interhemispheric transport of carbon by the oceans. *Global Biogeochem. Cycles* **13**(2), 287–305.

Nightingale, P. D., Malin, G., Law, C. S., Watson, A. J., Liss, P. S. and co-authors. 2000. In situ evaluation of air-sea gas exchange parameterizations using novel conservative and volatile tracers. *Global Biogeochem. Cycles* **14**(1), 373–387.

Nydal, R. 2000. Radiocarbon in the ocean. *Radiocarbon* **42**(1), 81–98.

Olsen, A., Wanninkhof, R., Trinanes, J. A. and Johannessen, T. 2005. The effect of wind speed products and wind speed-gas exchange relationships on interannual variability of the air-sea CO$_2$ gas transfer velocity. *Tellus* **57B**, 95–106.

Olsen, S. C. and Randerson, J. T. 2004. Differences between surface and column atmospheric CO$_2$ and implications for carbon cycle research. *J. Geophys. Res.* **109**, D02301, doi:10.1029/2003JD003968.

Orr, J. C., Maier-Reimer, E., Mikolajewicz, U., Monfray, P., Sarmiento, J. L. and co-authors. 2001. Estimates of anthropogenic carbon uptake from four three- dimensional global ocean models. *Global Biogeochem. Cycles* **15**(1), 43–60.

Orr, J. C., Fabry, V. J., Aumont, O., Bopp, L., Doney, S. C. and co-authors. 2005. Anthropogenic ocean acidification over the twenty-first century and its impact on calcifying organisms. *Nature* **437**(7059), 681–686.

Ostlund, H. G. and Stuiver, M. 1980. Geosecs Pacific radiocarbon. *Radiocarbon* **22**(1), 25–53.

Pacanowski, R. C., Dixon, K. and Rosati, A. 1993. The GFDL modular ocean model users guide. p. 46, Geophysical Fluid Dynamics Laboratory, Princeton, New Jersey.

Parker, R. L. and McNutt, M. K. 1980. Statistics for the one-norm misfit measure. *J. Geophys. Res.* **85**, 4429–4430.

Peacock, S. 2004. Debate over the ocean bomb radiocarbon sink: closing the gap. *Global Biogeochem. Cycles* **18**, GB2022.

Peacock, S., Maltrud, M. and Bleck, R. 2005. Putting models to the data test: a case study using Indian Ocean CFC-11 data. *Ocean Modelling* **9**(1), 1–22.

Peng, T. H., Broecker, W. S., Mathieu, G. G. and Li, Y. H. 1979. Radon evasion rates in the Atlantic and Pacific Oceans as determined during the Geosecs Program. *J. Geophys. Res.-Oceans Atmos.* **84**(NC5), 2471–2486.

Perrie, W., Zhang, W. Q., Ren, X. J., Long, Z. X. and Hare, J. 2004. The role of midlatitude storms on air-sea exchange of CO$_2$. *Geophys. Res. Lett.* **31**(9) L09306, doi:10.1029/2003GL019212.

Plattner, G. K., Joos, F. and Stocker, T. F. 2002. Revision of the global carbon budget due to changing air-sea oxygen fluxes. *Global Biogeochem. Cycles* **16**(4), art. no. 1096, doi:10.1029/2001GB001746.

Potter, C. S., Randerson, J. T., Field, C. B., Matson, P. A., Vitousek, P.

M. and co-authors. 1993. Terrestrial ecosystem production - a process model based on global satellite and surface data. *Global Biogeochem. Cycles* **7**(4), 811–841.

Prentice, I. C., Farquhar, G. D., Fasham, M. J. R., Goulden, M. L., Heimann, M. and co-authors. 2001. The carbon cycle and atmospheric carbon dioxide. In: *Climate Change 2001 : The Scientific Basis : Contribution of Working Group I to the Third Assessment Report of the Intergovernmental Panel on Climate Change* (eds.J. T. Houghton, Y. Ding, D. J. Griggs, M. Noguer, P. J. van der Linden, X. Da, K. Maskell and C. A. Johnson), Cambridge University Press, Cambridge, U.K. and New York, pp. 183–238.

Primeau, F. 2005. Characterizing transport between the surface mixed layer and the ocean interior with a forward and adjoint global ocean transport model. *J. Phys. Oceanogr.* **35**(4), 545–564.

Quay, P., King, S., White, D., Brockington, M., Plotkin, B. and co-authors. 2000. Atmospheric ^{14}CO: a tracer of OH concentration and mixing rates. *J. Geophys. Res.* **105**(D12), 15 147–15 166.

Quay, P., Sonnerup, R., Westby, T., Stutsman, J. and McNichol, A. 2003. Changes in the ^{13}C/^{12}C of dissolved inorganic carbon in the ocean as a tracer of anthropogenic CO$_2$ uptake. *Global Biogeochem. Cycles* **17**(1), art. no. 1004, doi:10.1029/2001GB001817.

Randerson, J. T., Enting, I. G., Schuur, E. A. G., Caldeira, K. and Fung, I. Y. 2002. Seasonal and latitudinal variability of troposphere $\triangle^{14}$CO$_2$: post bomb contributions from fossil fuels, oceans, the stratosphere, and the terrestrial biosphere. *Global Biogeochem. Cycles* **16**(4), art. no. 1112, doi:10.1029/2002GB001876.

Roy, T., Rayner, P., Matear, R. and Francey, R. 2003. Southern hemisphere ocean CO$_2$ uptake: reconciling atmospheric and oceanic estimates. *Tellus* **55B**, 701–710.

Rozanski, K., Levin, I., Stock, J., Falcon, R. E. G. and Rubio, F. 1995. Atmospheric ^{14}CO$_2$ variations in the Equatorial region. *Radiocarbon* **37**(2), 509–515.

Rubin, S. I. and Key, R. M. 2002. Separating natural and bomb-produced radiocarbon in the ocean: the potential alkalinity method. *Global Biogeochem. Cycles* **16**(4), 1105.

Sabine, C. L., Feely, R. A., Gruber, N., Key, R. M., Lee, K. and co-authors. 2004. The oceanic sink for anthropogenic CO$_2$. *Science* **305**(5682), 367–371.

Schlitzer, R. 2000. Applying the adjoint method for biogeochemical modeling: export of particulate organic matter in the world ocean. In: *Inverse Methods in Global Biogeochemical Cycles* (eds.Kasibhatla, P., Heimann, M., Rayner, P., Mahowald, N., Prinn, R. G. and Hartley, D. E.), American Geophysical Union, Washington, pp. 107–124.

Stammer, D., Ueyoshi, K., Köhl, A., Large, W. G., Josey, S. A. and co-authors. 2004. Estimating air-sea fluxes of heat, freshwater, and momentum through global ocean data assimilation. *J. Geophys. Res.* **109**, C05023, doi:10.1029/2003JC002082.

Stephens, C., Antonov, J. I., Conkright, M. E., Locranini, R. A., O'Brien, T. D. and co-authors. 2002. *World Ocean Atlas 2001, Volume 1: Temperature*, p. 167, US Government Printing Office, Washington.

Stuiver, M. and Becker, B. 1993. High-precision decadal calibration of the radiocarbon time scale, AD 1950-6000 BC. *Radiocarbon* **35**(1), 35–65.

Stuiver, M. and Ostlund, H. G. 1980. Geosecs Atlantic radiocarbon. *Radiocarbon* **22**(1), 1–24.

Stuiver, M. and Ostlund, H. G. 1983. Geosecs Indian-Ocean and Mediterranean radiocarbon. *Radiocarbon* **25**(1), 1–29.

Stuiver, M. and Polach, H. A. 1977. Reporting of C-14 data—discussion. *Radiocarbon* **19**(3), 355–363.

Stuiver, M. and Quay, P. D. 1981. Atmospheric ^{14}C changes resulting from fossil fuel CO_2 release and cosmic ray flux variability. *Earth Planet. Sci. Lett.* **53**(3), 349–362.

Suess, H. E. 1955. Radiocarbon concentration in modern wood. *Science* **122**(3166), 415–417.

Takahashi, T., Sutherland, S. C., Sweeney, C., Poisson, A., Metzl, N. and co-authors. 2002. Global sea-air CO_2 flux based on climatological surface ocean pCO_2, and seasonal biological and temperature effects. *Deep-Sea Res.* **49**(9–10), 1601–1622.

Tang, W. and Liu, W. T. 1996. Equivalent Neutral Wind. pp. 20, JPL Publication 96–17, Pasadena.

Tans, P. P., Berry, J. A. and Keeling, R. F. 1993. Oceanic ^{13}C/^{12}C observations: a new window on ocean CO_2 uptake. *Global Biogeochem. Cycles* **7**(2), 353–368.

Tans, P. P., Dejong, A. F. M. and Mook, W. G. 1979. Natural atmospheric C-14 variation and the Suess Effect. *Nature* **280**(5725), 826–827.

Tans, P. P., Fung, I. Y. and Takahashi, T. 1990. Observational constraints on the global atmospheric CO_2 Budget. *Science* **247**(4949), 1431–1438.

Thompson, M. V. and Randerson, J. T. 1999. Impulse response functions of terrestrial carbon cycle models: method and application. *Glob. Change Biol.* **5**(4), 371–394.

Toggweiler, J. R., Dixon, K. and Bryan, K. 1989. Simulations of radiocarbon in a coarse-resolution world ocean model .1. Steady state prebomb distributions. *J. Geophys. Res.* **94**(C6), 8217–8242.

Trolier, M., White, J. W. C., Tans, P. P., Masarie, K. A. and Gemery, P. A. 1996. Monitoring the isotopic composition of atmospheric CO_2: measurements from the NOAA Global Air Sampling Network. *J. Geophys. Res.* **101**(D20), 25 897–25 916.

Turney, D. E., Smith, W. C. and Banerjee, S. 2005. A measure of near-surface fluid motions that predicts air-water gas transfer in a wide range of conditions. *Geophys. Res. Lett.* **32**(4).

Van Scoy, K. A., Morris, K. P., Robertson, J. E. and Watson, A. J. 1995. Thermal skin effect and the air-sea flux of carbon dioxide: a seasonal high-resolution estimate. *Global Biogeochem. Cycles* **9**(2), 253–262.

Vogel, J. C. 1971. Pretoria radiocarbon dates I. *Radiocarbon* **13**(2), 378–394.

Walsh, J. 1978. A data set on northern hemisphere sea ice extent, 1953-1976. pp. 49–51, World Data Center for Glaciology (Snow and Ice), Report GD-2,.

Wanninkhof, R. 1992. Relationship between wind-speed and gas-exchange over the ocean. *J. Geophys. Res.* **97**(C5), 7373–7382.

Wanninkhof, R. and McGillis, W. R. 1999. A cubic relationship between air-sea CO_2 exchange and wind speed. *Geophys. Res. Lett.* **26**(13), 1889–1892.

Wanninkhof, R., Sullivan, K. F. and Top, Z. 2004. Air-sea gas transfer in the Southern Ocean. *J. Geophys. Res.* **109**(C8) C08519, doi:10.1029/2003JC001767.

Ward, B., Wanninkhof, R., McGillis, W. R., Jessup, A. T., DeGrandpre, M. D. and co-authors. 2004. Biases in the air-sea flux of CO_2 resulting from ocean surface temperature gradients. *J. Geophys. Res.* **109**(C8) C08508, doi:10.1029/2003JC001800.

Weiss, R. F. 1974. Carbon dioxide in water and seawater: solubility of a non-ideal gas. *Mar. Chem.* **2**, 203–215.

Weiss, R. F. and Price, B. A. 1980. Nitrous oxide solubility in water and seawater. *Mar. Chem.* **8**(4), 347–359.

Woolf, D. K. 2005. Parametrization of gas transfer velocities and sea-state-dependent wave breaking. *Tellus* **57B**, 87–94.

Zhang, J., Quay, P. D. and Wilbur, D. O. 1995. Carbon isotope fractionation during gas-water exchange and dissolution of CO_2. *Geochim. Cosmochim. Acta* **59**(1), 107–114.

Zhao, D., Toba, Y., Suzuki, Y. and Komori, S. 2003. Effect of wind waves on air-sea gas exchange: proposal of an overall CO_2 transfer velocity formula as a function of breaking-wave parameter. *Tellus* **55B**, 478–487.

Zwally, H. J., Comiso, J., Parkinson, C., Campbell, W., Carsey, F. and co-authors. 1983. Antarctic Sea Ice, 1973–1976: satellite passive microwave observations, pp. 206, NASA.